ELECTRONIC SUPPLEMENTARY INFORMATION

Salicylidene-based dual-responsive `turn on´ fluorometric chemosensors for the selective detection of Zn^{2+}, Al^{3+} and F^{-} ions: theoretical investigation and applications in the live cell imaging of zebrafish larvae and molecular logic gate operation

Abbas Khaja Raees Ahmed,[a] Ramalingam Gajendhiran,[a] Sivaraj Mithra,[b] Seepoo Abdul Majeed,[b] Azeez Sait Sahul Hameed,[b] Rajakkani Paulpandiyan,[c] Subbaiah Maniyammai,[d] Gurusamy Thangavelu Senthil Andavan,[d] MohamedHanifa NizamMohideen,[e] and Aziz Kalilur Rahiman*[a]

[a]Post-Graduate and Research Department of Chemistry, The New College, University of Madras, Chennai - 600 014, India
[b]Department of Zoology and Aquatic Animal Health Laboratory, C. Abdul Hakeem College, Melvisharam - 632 509, India
[c]Research Department of Chemistry, VHNSN College, Virudhunagar - 626 001, India
[d]Department of Chemistry, SRM Institute of Science and Technology, Kattankulathur, Chennai - 603 203, India
[e]Post-Graduate and Research Department of Physics, The New College, University of Madras, Chennai - 600 014, India
**E-mail address: akrahmanjkr@gmail.com; kalilurrahiman@thenewcollege.edu.in*

Table S1 Crystal data and structure refinement details for chemosensors R1 and R3

Empirical Formula	$C_{15}H_{12}N_4Br_2O_3$ (R1)	$C_{21}H_{28}N_4O_6S$ (R3)
Formula weight	456.11	464.53
Crystal system	Orthorhombic	Monoclinic
Space group	*Pbcn*	$P2_1/n$
Temperature (K)	293(2)	273.15
a (Å)	3.8523(10)	9.5427(8)
b (Å)	12.8505(4)	18.3688(16)
c (Å)	36.4286(11)	14.1766(12)
α (°)	90	90
β (°)	90	95.890(3)
γ (°)	90	90
Volume ($Å^3$)	1803.36(9)	2471.9(4)
Z/Z'	4/0.5	4/1
Calculated density (mg m^{-3})	1.680	1.248
Absorption coefficient (mm^{-1})	4.515	0.172
Crystal size (mm)	0.42 × 0.21 × 0.15	0.24 × 0.18 × 0.12
F(000)	896	984
θ Range for data collection (°)	4.472 to 57.526	4.434 to 54.258
Limiting indices	$-3 \le h \le 5$, $-17 \le k \le 17$, $-49 \le l \le 49$	$-11 \le h \le 12$, $-23 \le k \le 23$, $-18 \le l \le 18$
Reflections collected	27,732	48,905
Independent reflections	2351 [R(int) = 0.0462, R(sigma) = 0.0272]	5458 [R(int) = 0.0629, R(sigma) = 0.0376]
Data/restraints/parameters	2351/0/118	2423/0/181
Goodness of fit on F^2	1.198	1.024
Final R indices	R1 = 0.0579, wR2 = 0.1206	R1 = 0.0597, wR2 = 0.1561
R indices (all data)	R1 = 0.0674, wR2 = 0.1246	R1 = 0.0769, wR2 = 0.1715
Largest diff. peak and hole (e.$Å^{-3}$)	0.79 and −0.66	0.46 and −0.33

Table S2 Selected bond length (Å), bond angle (°) and tortional angle (°) values of the chemosensors R1 and R3

Bonds length (Å)	R1	R3
O(1)–C(6)	1.226(7)	1.230(2)
N(1)–C(5)	1.277(6)	1.273(3)
N(2)–C(6)	1.354(5)	1.357(3)
N(1)–N(2)	1.364(5)	1.372(3)
C(7)–C(8)	1.377(6)	1.371(4)
O(2)–C(3)	1.355(6)	1.356(2)
Bond angle (°)		
C(6)–N(2)–N(1)	118.9(4)	119.7(17)
C(5)– N(1)–N(2)	117.1(4)	116.7(17)
O(1)–C(6)–N(2)	123.3(3)	121.2(18)
N(2A)–C(6)–N(2)	113.4(6)	115.0(18)
Torsional angle (°)		
C(5)–N(1)–N(2)–C(6)	178.6(4)	–171.3(19)
N(2)–N(1)–C(5)–C(4)	–179.2(5)	–179.8(18)
N(1)–N(2)–C(6)–O(1)	–1.0(6)	178.2(19)

Table S3 Hydrogen bonding geometry for the chemosensor R1 (Å and °)

D–H···A	d(D–H)	d(H···A)	d(D···A)	<D–H···A
O(2)–H(2B)···N(1)	0.85(7)	1.89(7)	2.625(5)	145(7)

Table S4 Hydrogen bonding geometry for the chemosensor R3 (Å and °)

D–H···A	d(D–H)	d(H···A)	d(D···A)	<D–H···A
O(2)–H(2)···O(3)	0.82	2.17	2.6310	115
O(2)–H(2)···O(4)$^{(i)}$	0.82	1.99	2.7155	148'
N(2)–H(2A)···O(1)$^{(ii)}$	0.85	2.04	2.8869	176
N(2A)–H(2AA)···N(1)	0.86	2.26	2.6114	105
N2A–H(2AA)···O(4)$^{(iii)}$	0.86	2.37	3.1387	150'
O(2A)–H(2AB)···N(1A)	0.82	1.91	2.6306	146
C(5A)–H(5A)···O(4)$^{(iii)}$	0.93	2.45	3.2197	153
C(8A)–H(8A)···O(2)$^{(iv)}$	0.93	2.55	3.4218	156
C(11)–H(11C)···O(2A)$^{(v)}$	0.96	2.50	3.2813	139
C(12)–H(12B)···O(3A)$^{(v)}$	0.96	2.57	3.4809	158
C(12)–H(12C)···O(2)$^{(vi)}$	0.96	2.58	3.3108	133
O(2)–H(2)···O(3)	0.82	2.17	2.6310	115

Symmetry code: (i) 1 + x, y, –1 + z (ii) 2 – x , –y , –z
(iii) 1/2 + x, 1/2 – y, –1/2 + z (iv) –1/2 + x, 1/2 – y, 1/2 + z
(v) 1 – x, –y ,1 – z (vi) –1 + x, y ,1 + z

Table S5 Selected bond length (Å) values of the chemosensors R1 and R2, and upon interaction with Zn^{2+} and Al^{3+} cations (R1 + Zn^{2+}, R1 + Al^{3+} and R2 + Zn^{2+}) calculated using theoretical studies

Parameters	R1	R1 + Zn^{2+}	R1 + Al^{3+}	R2	R2 + Zn^{2+}
C5–O8	1.386	1.323	1.337	1.384	1.299
C7–N9	1.305	1.458	1.470	1.306	1.425
C11–O12	1.245	1.421	1.452	–	–
C14–N15	1.306	1.457	1.469	–	–
C21–O22	1.397	1.513	1.566	–	–
C11–S24	–	–	–	1.709	1.825
C16–O21	–	–	–	1.396	1.293
N13–C14	–	–	–	1.307	1.429

Table S6 Selected bond length (Å) values of the chemosensors R3 and R4, and upon interaction with Zn^{2+} and Al^{3+} cations (R3 + Zn^{2+}, R3 + Al^{3+} and R4 + Zn^{2+}) calculated using theoretical studies

Parameters	R3	R3 + Zn^{2+}	R3 + Al^{3+}	R4	R4 + Zn^{2+}
C5–O8	1.386	1.369	1.342	1.373	1.361
C7–N9	1.305	1.438	1.453	1.296	1.424
C11–O22	1.241	1.379	1.382	–	–
C16–O21	1.397	1.315	1.330	–	–
N13–C14	1.306	1.440	1.449	–	–
C13–S16	–	–	–	1.709	1.890
C19–O24	–	–	–	1.384	1.314
N15–C17	–	–	–	1.299	1.436

Table S7 Selected bond length (Å) values of the chemosensors R1 and R2, and upon interaction with F^- anion (R1 + F^- and R2 + F^-) calculated using theoretical studies

Parameters	R1	R1 + F^-	R2	R2 + F^-
N10–H31	1.023	1.520	–	–
N13–H30	1.018	1.022	–	–
O8–H36	0.980	0.971	–	–
O22–H25	0.978	0.971	–	–
N10–H29	–	–	1.026	1.025
N12–H30	–	–	1.018	1.522
O8–H28	–	–	0.980	0.970

Table S8 Selected bond length (Å) values of the chemosensors R3 and R4, and upon interaction with F^- anion (R3 + F^- and R4 + F^-) calculated using theoretical studies

Parameters	R3	R3 + F^-	R4	R4 + F^-
N10–H31	1.023	1.023	–	–
N12–H32	1.018	1.526	–	–
O8–H30	0.980	.970	–	–
O21–H36	0.978	0.971	–	–
N12–H36	–	–	1.020	1.509
N14–H37	–	–	1.011	1.025
O8–H33	–	–	0.980	0.970
O21–H42	–	–	0.978	0.970

Table S9 Selected bond angle (º) values of the chemosensors R1 and R2, and upon interaction with Zn^{2+} and Al^{3+} cations (R1 + Zn^{2+}, R1 + Al^{3+} and R2 + Zn^{2+}) calculated using theoretical studies

Parameters	R1	R1 + Zn^{2+}	R1 + Al^{3+}	R2	R2 + Zn^{2+}
C7–N9–N10	115.923	124.752	123.538	115.431	118.512
N10–C11–O12	127.693	120.066	120.884	–	–
N13–C11–O12	119.957	122.879	122.412	–	–
N13–N14–C15	122.258	117.624	118.378	–	–
N10–C11–S24	–	–	–	128.504	127.891
N12–C11–S24	–	–	–	119.262	117.775
N12–N13–C14	–	–	–	121.922	120.111

Table S10 Selected bond angle (º) values of the chemosensors R3 and R3, and upon interaction with Zn^{2+} and Al^{3+} cations (R3 + Zn^{2+}, R3 + Al^{3+} and R4 + Zn^{2+}) calculated using theoretical studies

Parameters	R3	R3 + Zn^{2+}	R3 + Al^{3+}	R4	R4 + Zn^{2+}
C7–N9–N10	115.923	125.047	123.173	–	–
N10–C11–O22	127.693	120.074	120.073	–	–
N12–C11–O22	119.957	123.011	123.627	–	–
N12–N13–C14	122.258	117.280	119.948	–	–
C7–N11–N12	–	–	–	115.578	121.636
N12–C13–S16	–	–	–	128.065	124.254
N14–C13–S16	–	–	–	119.318	120.740
N14–N15–C17	–	–	–	121.406	117.663

Table S11 Selected bond angle (º) values of the chemosensors R1 and R2, and upon interaction with F^- anion (R1 + F^- and R2 + F^-) calculated using theoretical studies

Parameters	R1	R1 + F^-	R2	R2 + F^-
C5–O8–H36	112.254	114.748	–	–
C21–O22–H25	112.690	112.504	–	–
N9–N10–H31	122.871	128.497	–	–
N14–N13–H30	123.586	121.064	–	–
C5–O8–H28	–	–	112.460	114.071
C16–O21–H34	–	–	112.696	112.626
N9–N10–H29	–	–	121.962	128.282
N13–N12–H30	–	–	123.381	123.932

Table S12 Selected bond angle (º) values of the chemosensors R3 and R4, and upon interaction with F^- anion (R3 + F^- and R4 + F^-) calculated using theoretical studies

Parameters	R3	R3 + F^-	R4	R4 + F^-
C5–O8–H30	112.254	112.677	–	–
C16–O21–H36	112.690	109.713	–	–
N9–N10–H31	122.871	121.216	–	–
N13–N12–H32	123.586	129.076	–	–
C5–O8–H33	–	–	109.086	108.652
C19–O24–H42	–	–	109.118	109.057
N11–N12–H36	–	–	121.078	127.558
N15–N14–H37	–	–	122.599	123.511

Table S13 Absolute energies (in Hartree units) of the chemosensors (R1–R4), R1–R4 + Zn^{2+}, R2/R4 + Al^{3+} and R1–R4 + F^{-} calculated using theoretical studies

Parameters	Absolute energy
R1	–1049.585
R1 + Zn^{2+}	–1179.629
R1 + Al^{3+}	–1252.502
R1 + F^{-}	–1271.397
R2	– 984.461
R2 + Zn^{2+}	–1235.634
R2 + F^{-}	–1494.372
R3	–938.295
R3 + Zn^{2+}	–1311.755
R3 + Al^{3+}	–1484.632
R3 + F^{-}	–1432.082
R4	–1055.222
R4 + Zn^{2+}	–1246.642
R4 + F^{-}	–1355.059

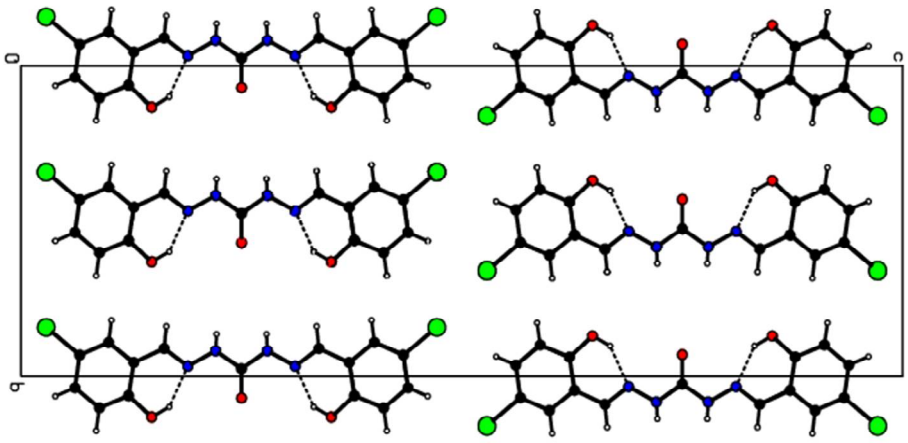

Fig. S1 Crystal packing diagram of the chemosensor R1 along the crystallographic *a*-axis.

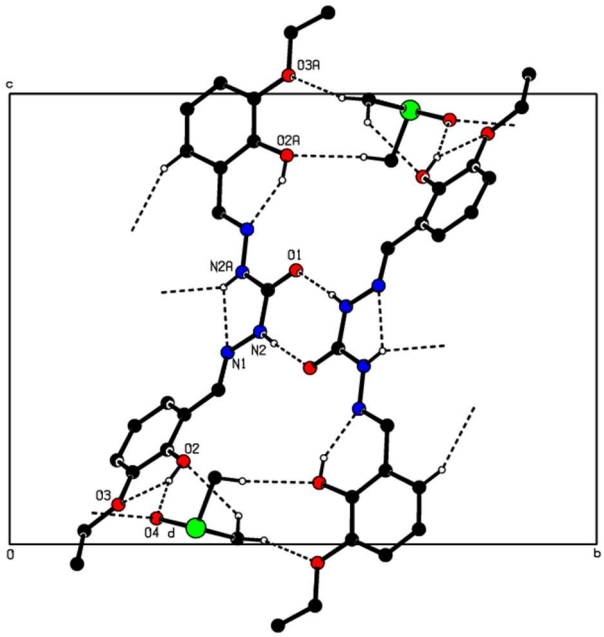

Fig. S2 Crystal lattice packing diagram of the chemosensor R3 showing O–H···O and O–H···N intramolecular hydrogen bonding interaction along *a*-axis.

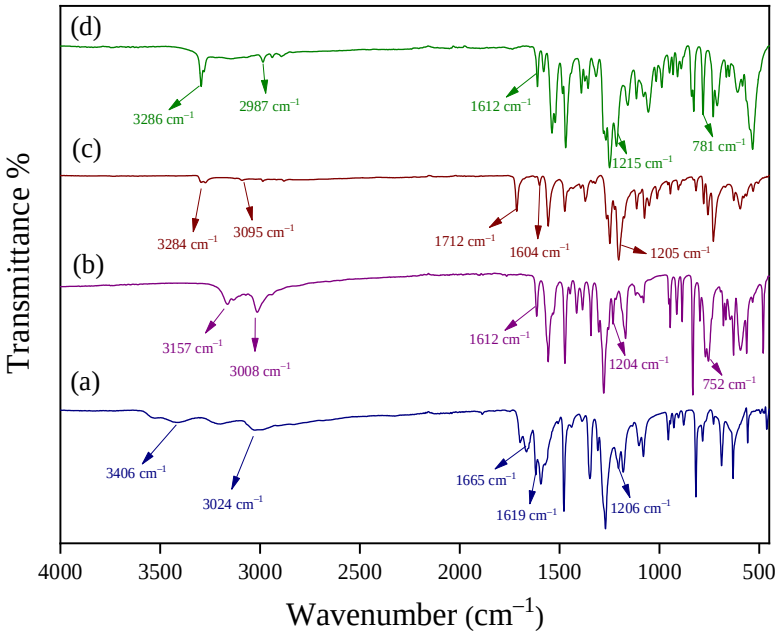

Fig. S3 FT IR spectra of the chemosensors R1 (a), R2 (b), R3 (c) and R4 (d).

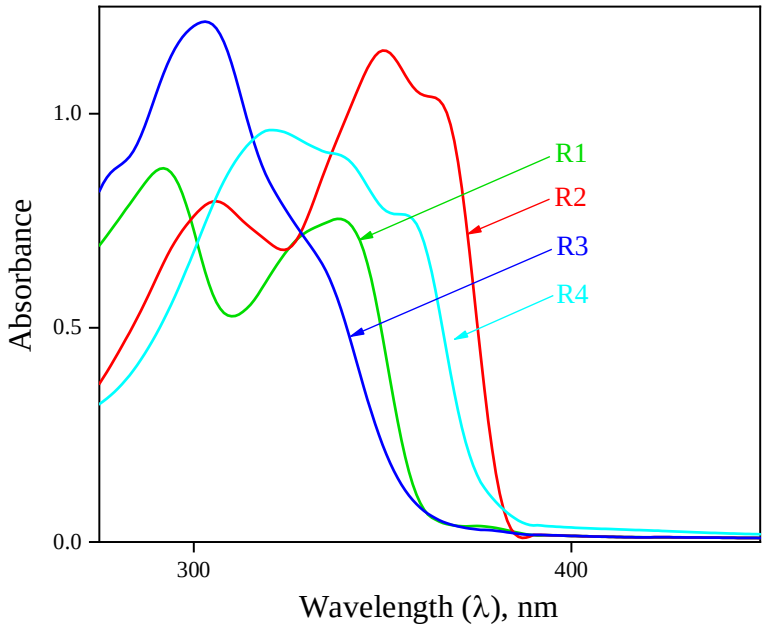

Fig. S4 UV-Vis spectra of the chemosensors (R1–R4).

(a)

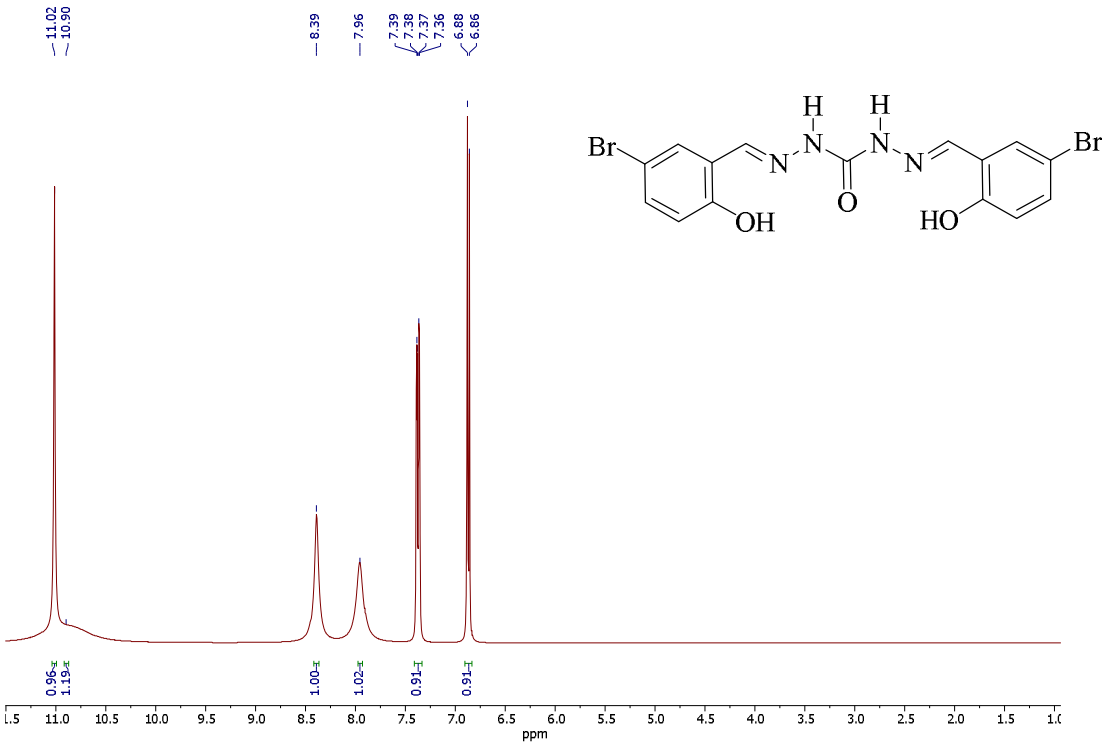

(b)

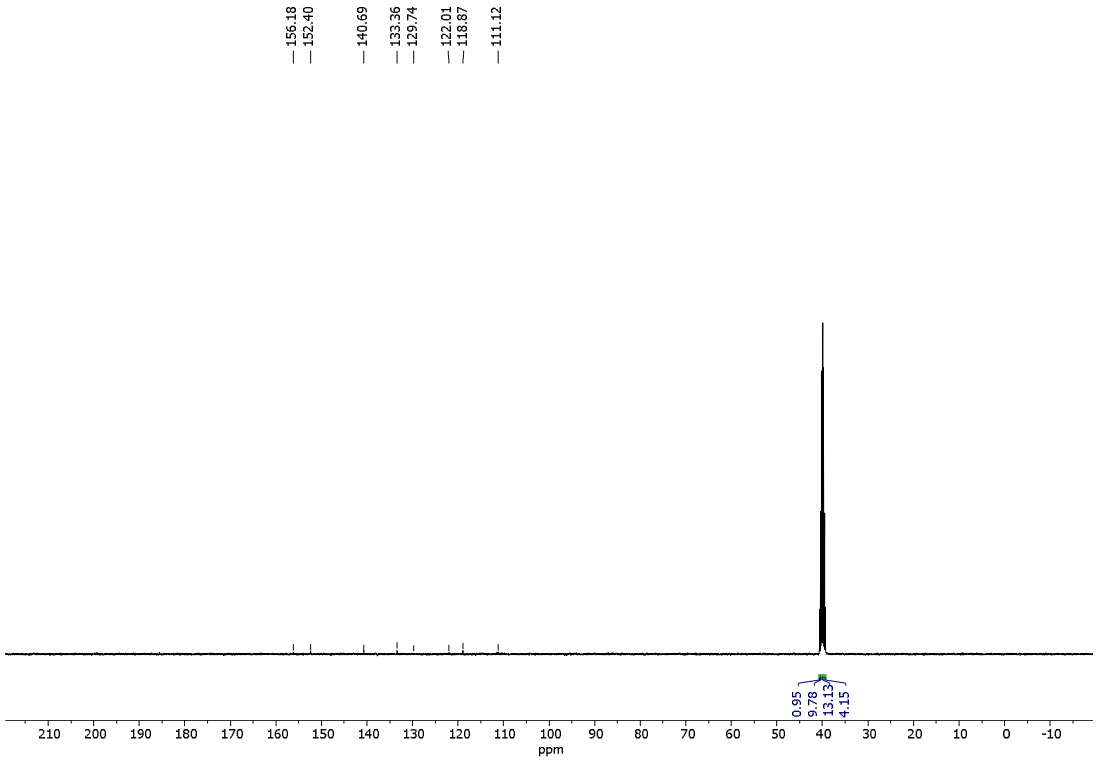

Fig. S5 ^{1}H (a) and ^{13}C (b) NMR spectra of the chemosensor R1.

(a)

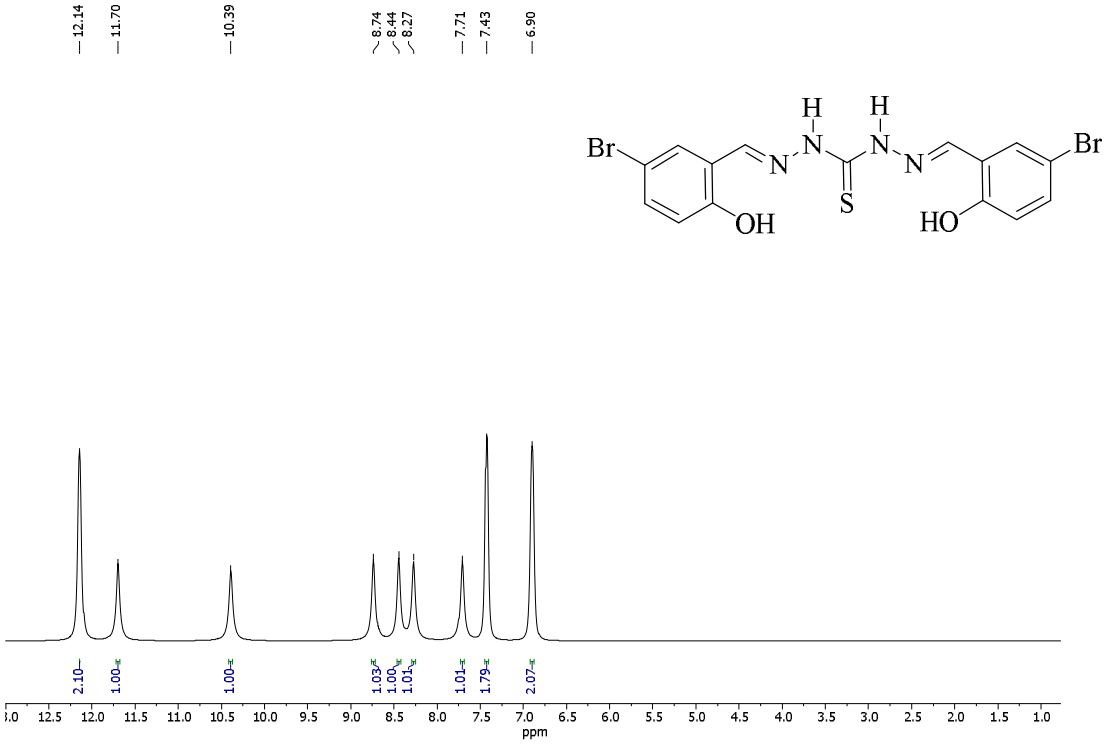

(b)

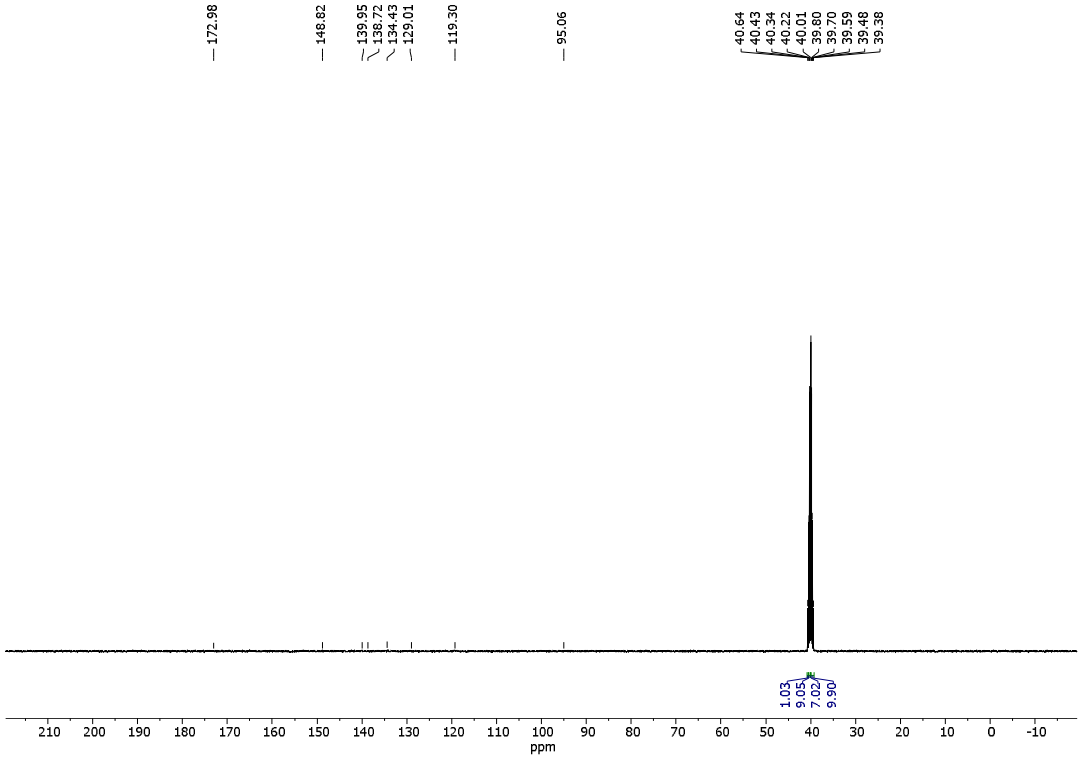

Fig. S6 ^{1}H (a) and ^{13}C (b) NMR spectra of the chemosensor R2.

(a)

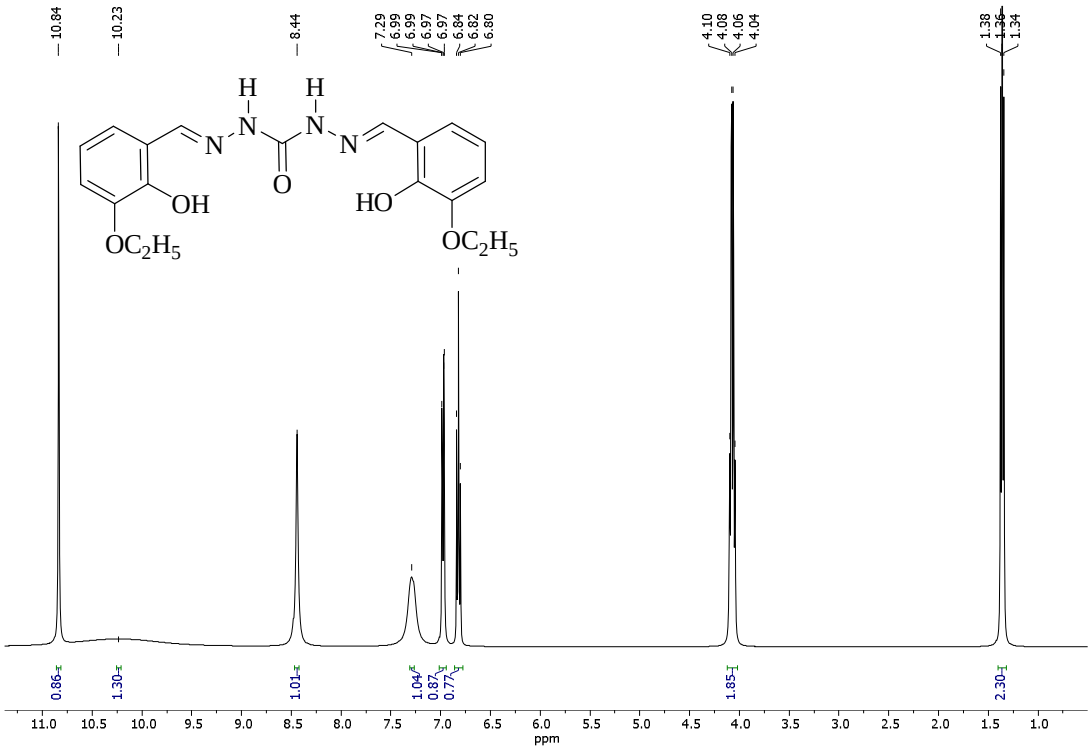

(b)

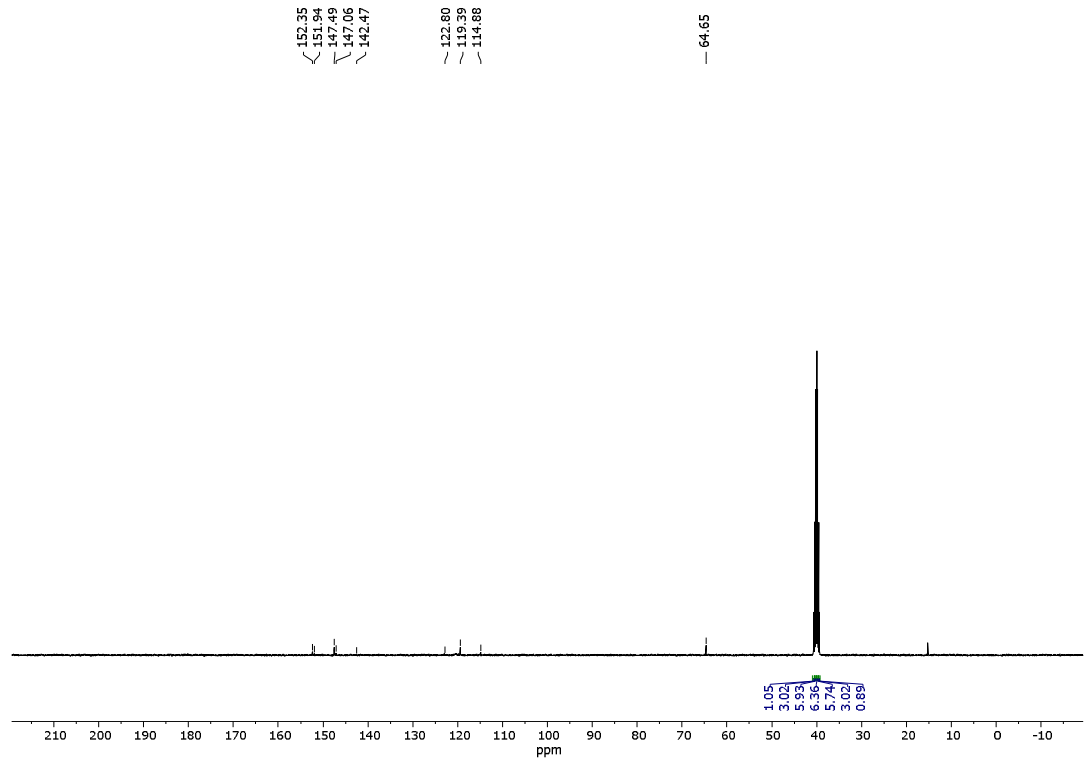

Fig. S7 ^{1}H (a) and ^{13}C (b) NMR spectra of the chemosensor R3.

(a)

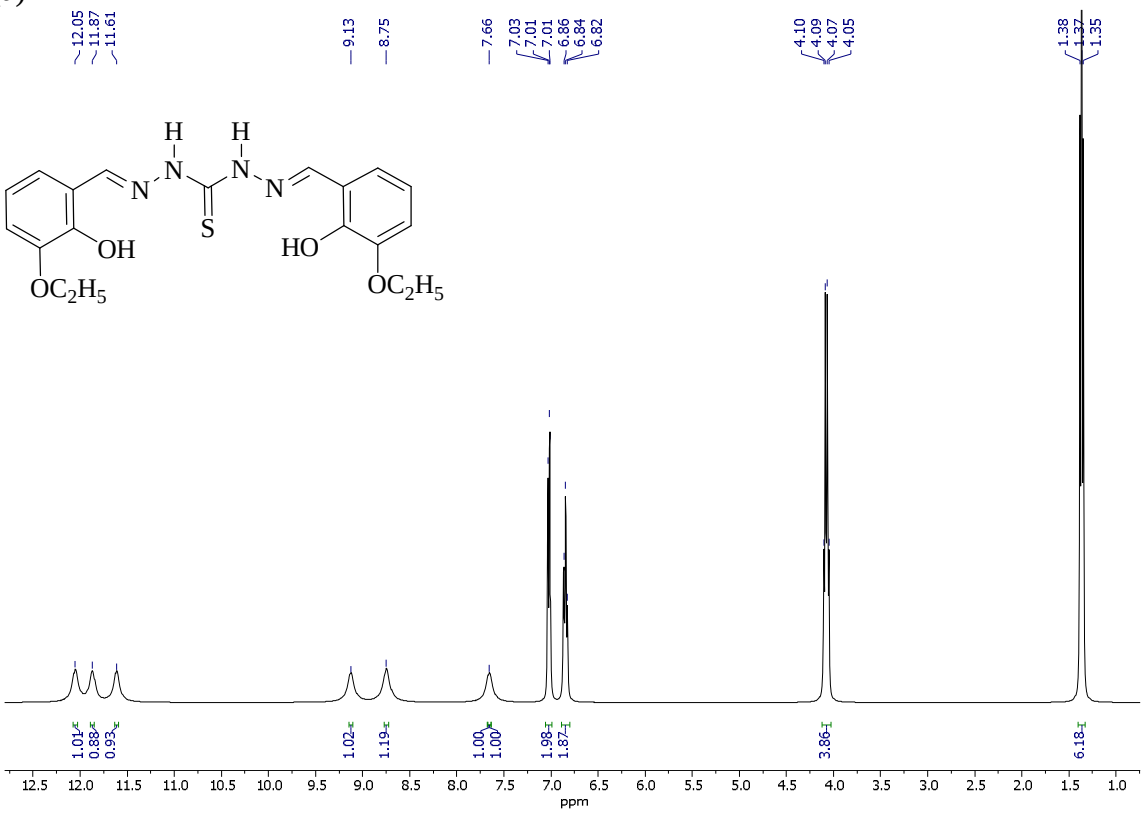

(b)

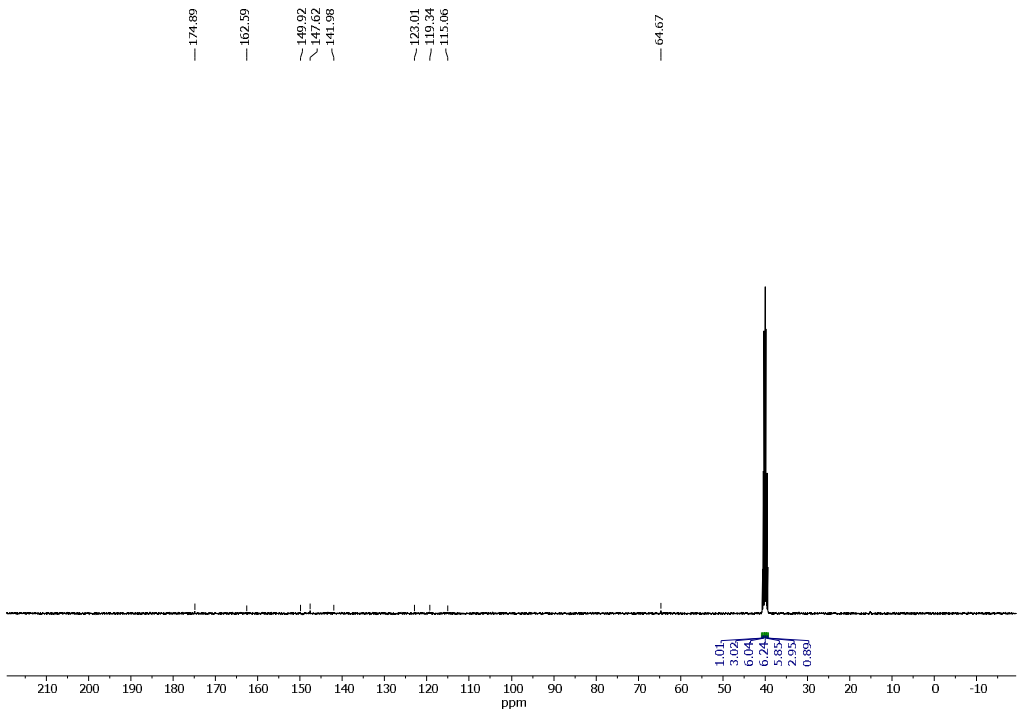

Fig. S8 ^{1}H (a) and ^{13}C (b) NMR spectra of the chemosensor R4.

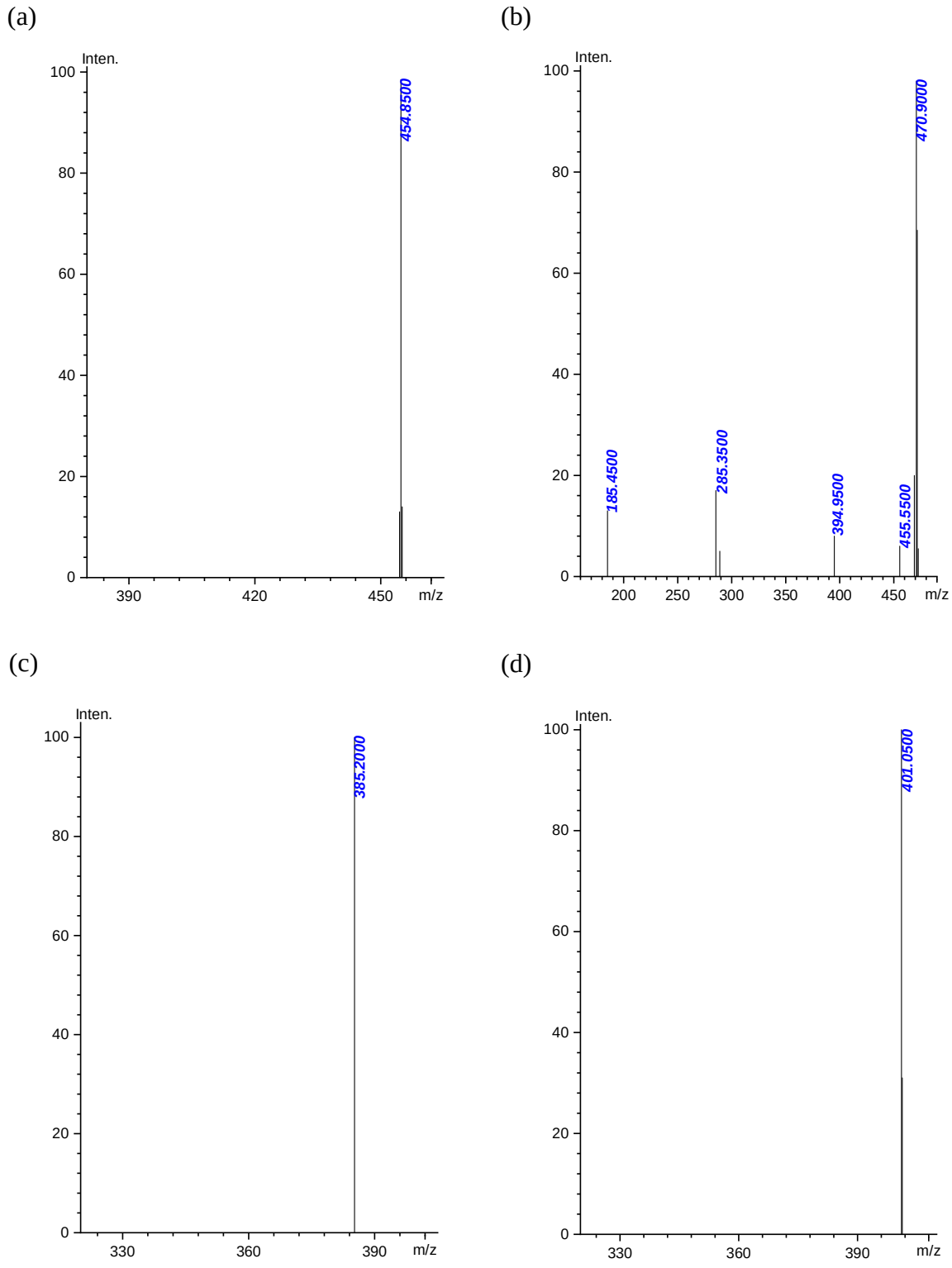

Fig. S9 LC-MS spectra of the chemosensors R1 (a), R2 (b), R3 (c) and R4 (d).

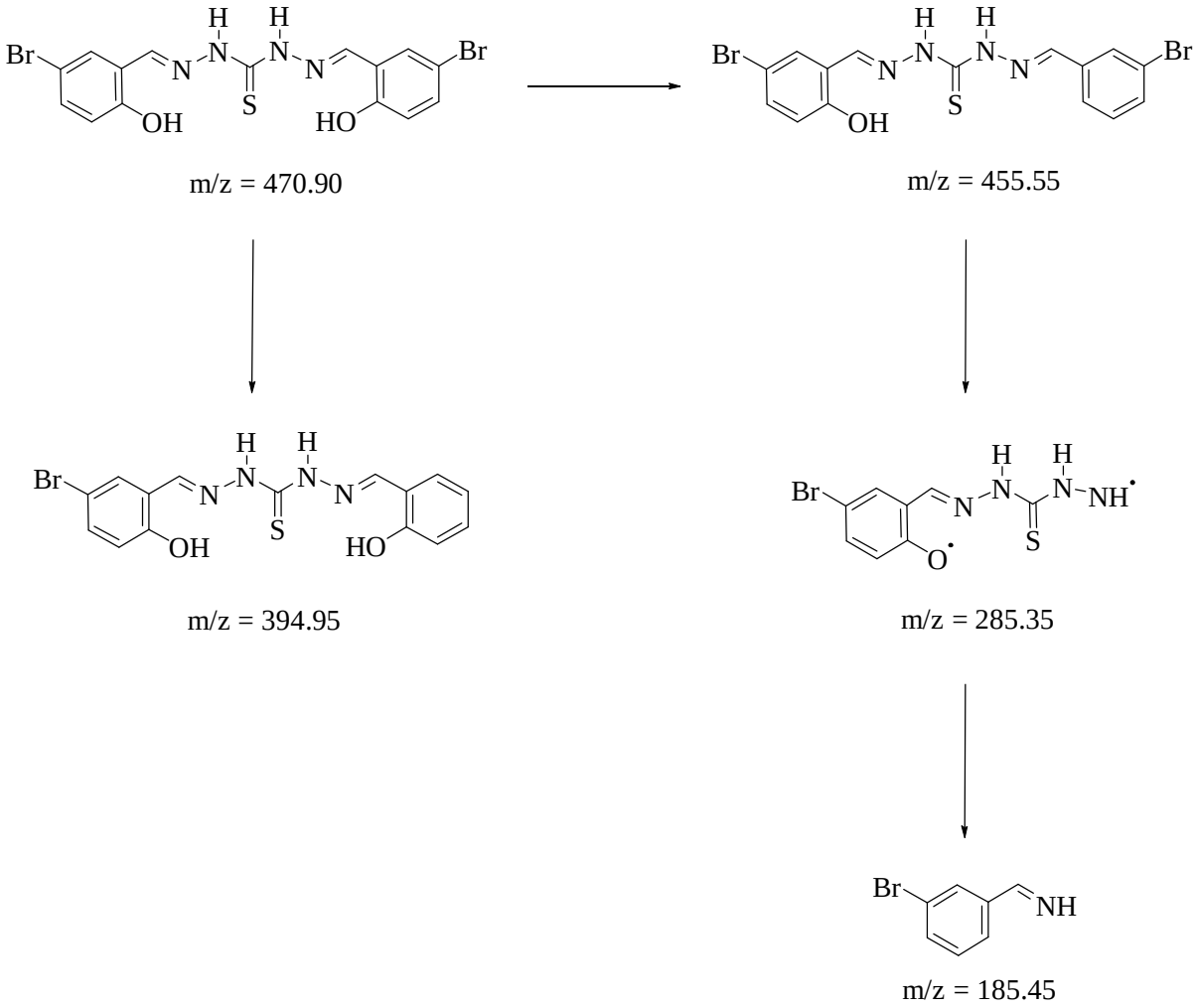

Fig. S10 Mass fragmentation pattern of the chemosensor R2.

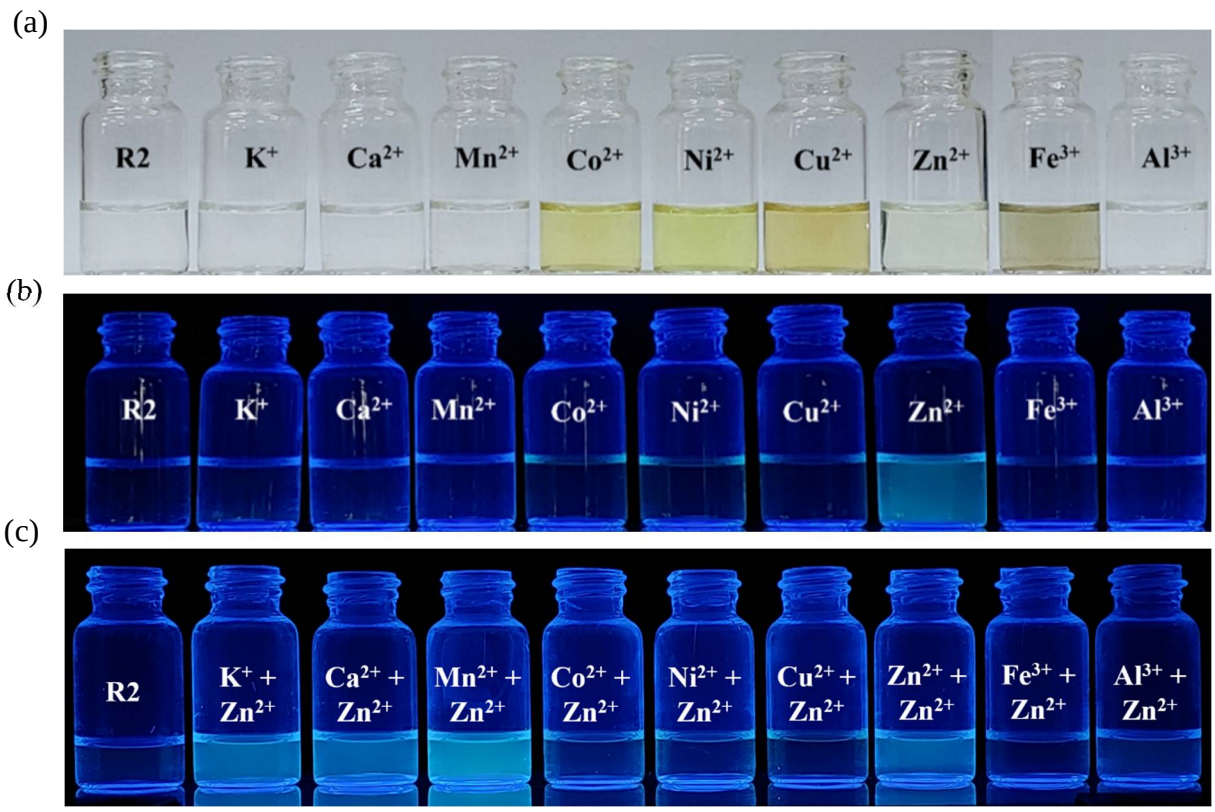

Fig. S11 Visual responses of R2 upon addition of different metal ions under ambient (a) and UV light (b) conditions, and towards Zn^{2+} cation in the presence of various competing metal ions under UV light condition (c), in CH_3CN:DMSO (v/v 9:1).

Fig. S12 Visual responses of R3 upon addition of different metal ions under ambient (a) and UV light (b) conditions, and towards Zn^{2+} (c) and Al^{3+} (d) cations in the presence of various competing metal ions under UV light condition, in CH_3CN:DMSO (v/v 9:1).

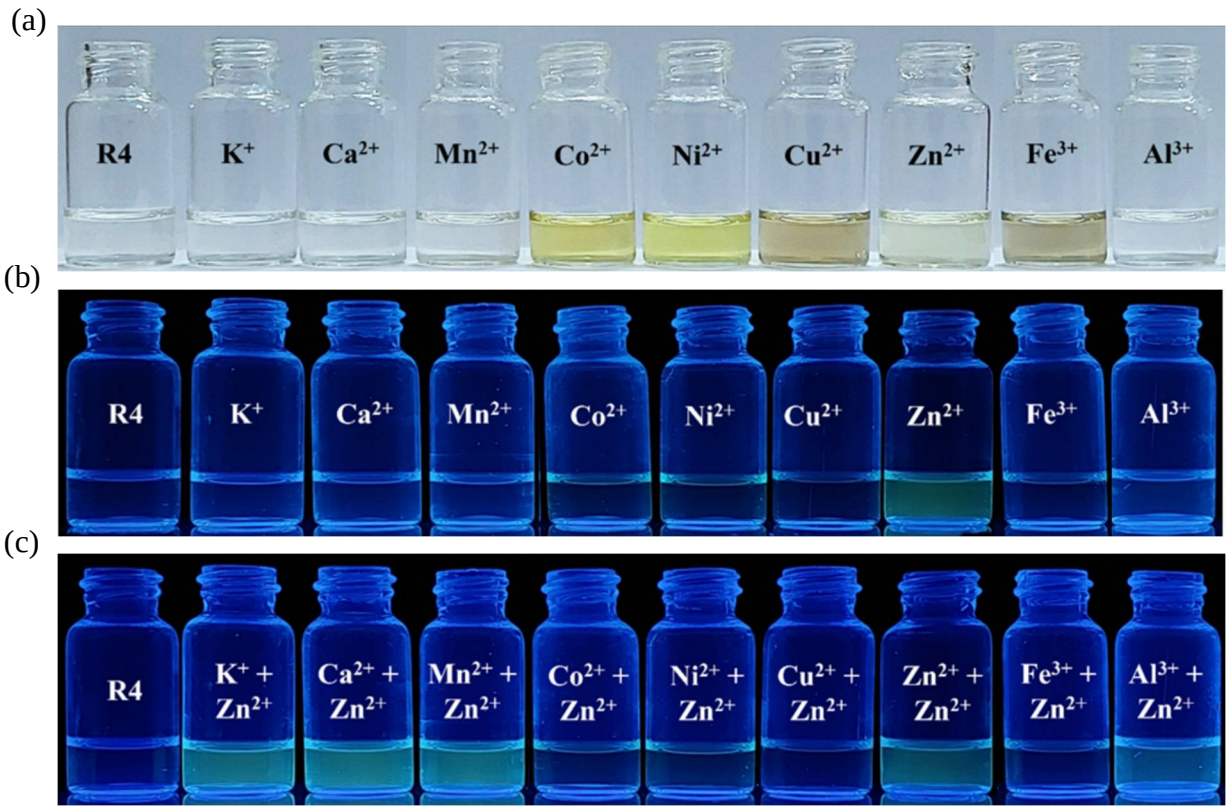

Fig. S13 Visual responses of R4 upon addition of different metal ions under ambient (a) and UV light (b) conditions, and towards Zn^{2+} cation in the presence of various competing metal ions under UV light condition (c), in CH_3CN:DMSO (v/v 9:1).

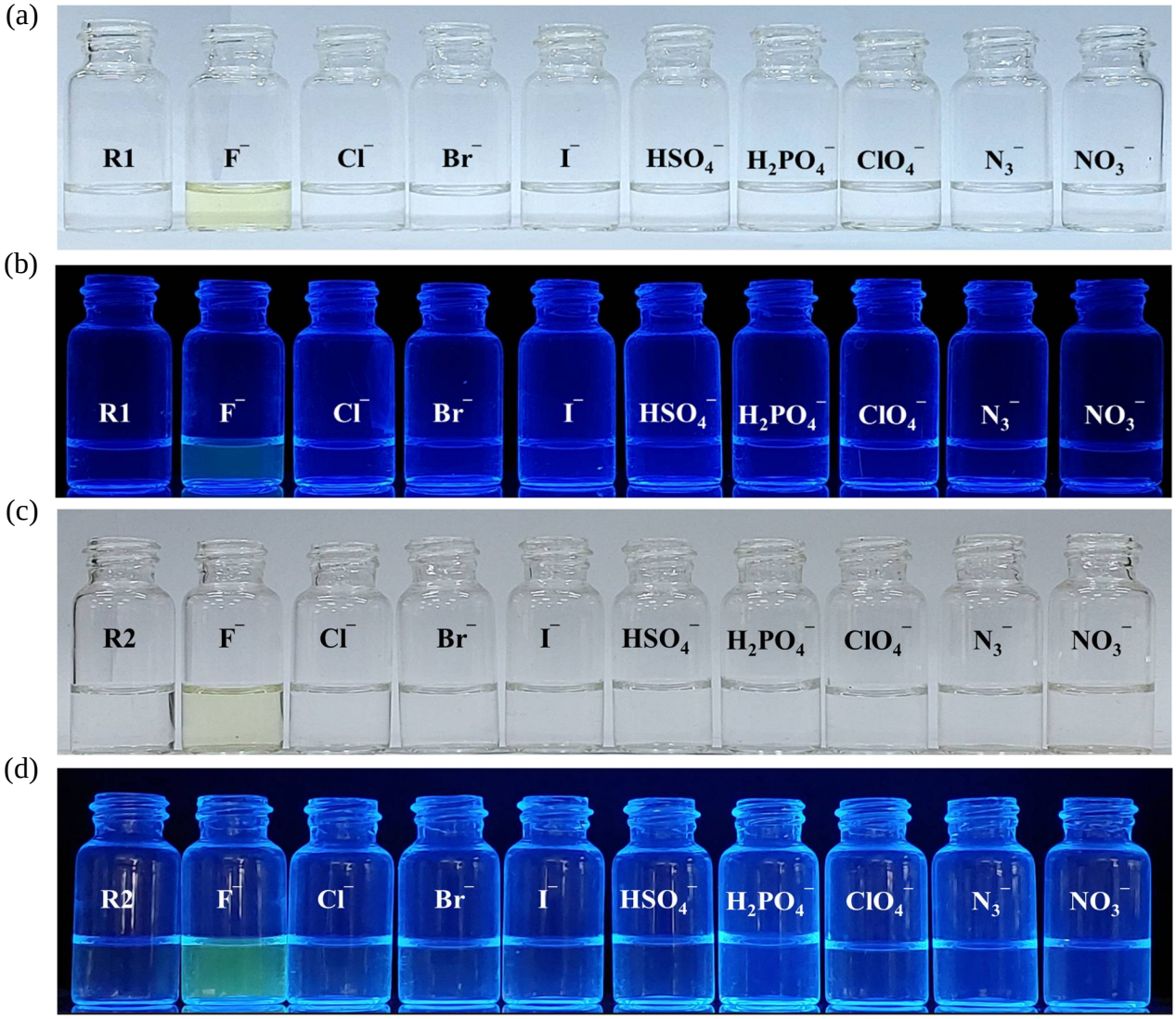

Fig. S14 Visual responses of R1 upon addition of different anions under ambient (a) and UV light (b) conditions, and R2 upon addition of different anions under ambient (c) and UV light (d) conditions, in CH_3CN:DMSO (v/v 9:1).

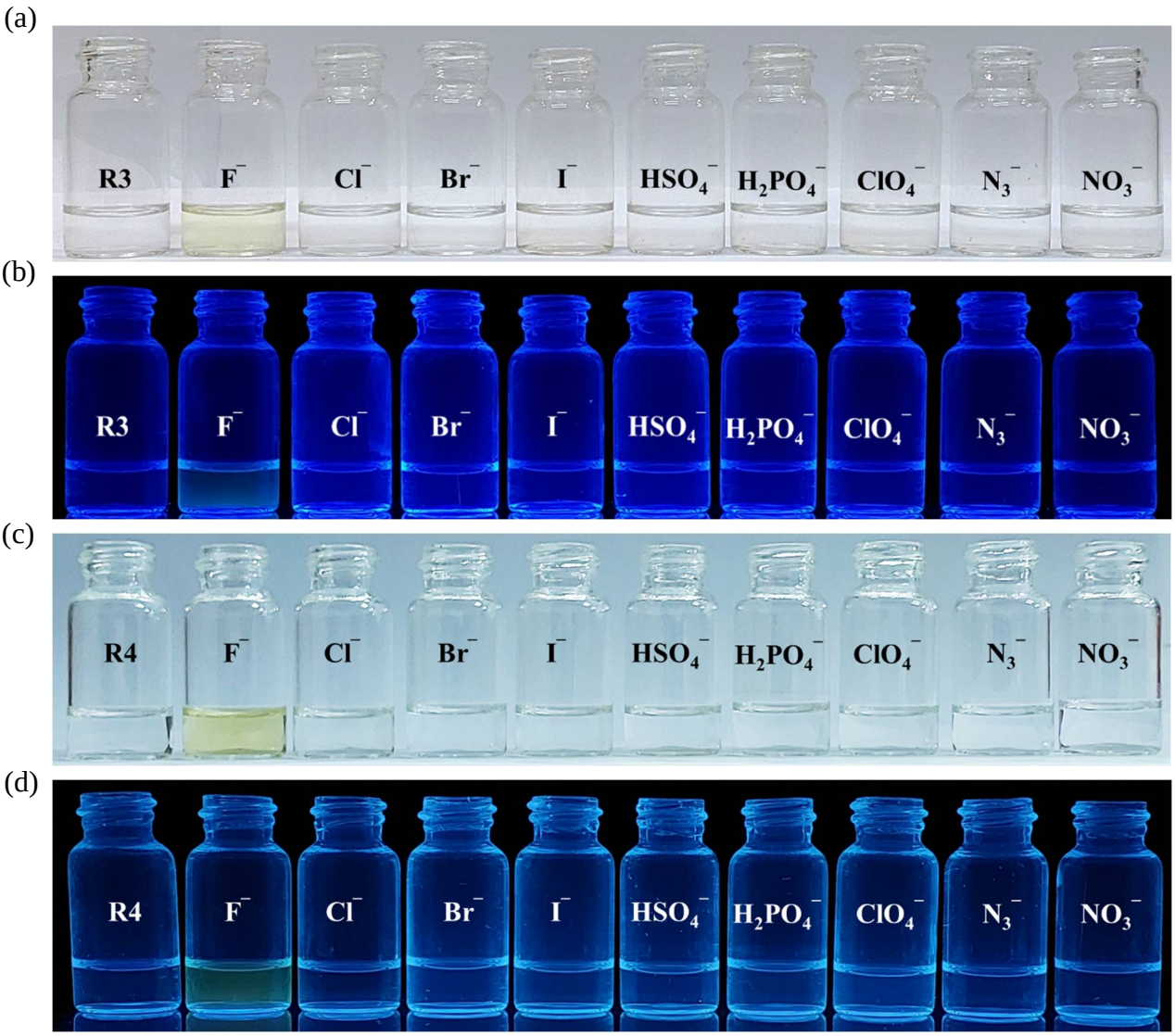

Fig. S15 Visual responses of R3 upon addition of different anions under ambient (a) and UV light (b) conditions, and R4 upon addition of different anions under ambient (c) and UV light (d) conditions, in CH_3CN:DMSO (v/v 9:1).

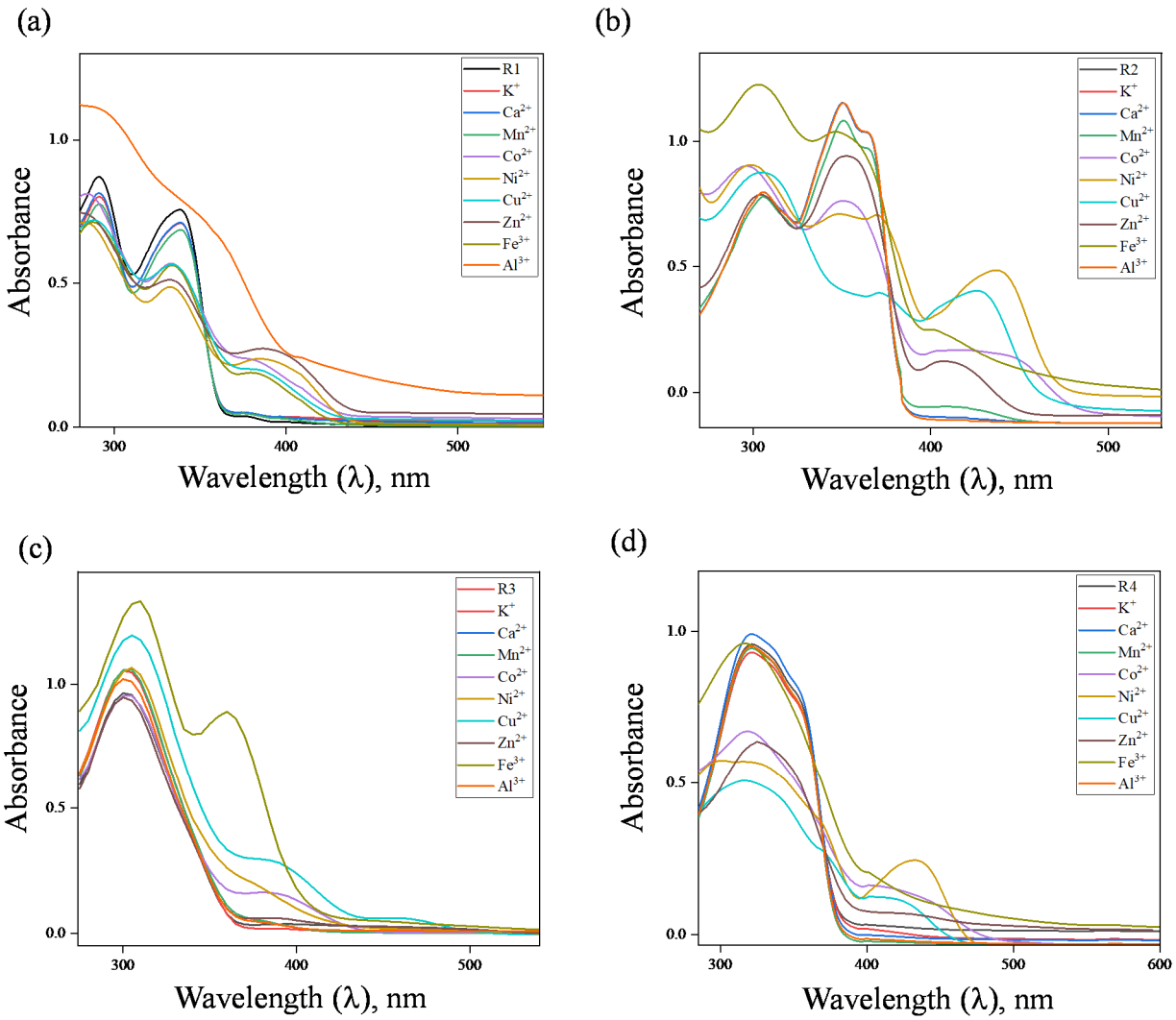

Fig. S16 Absorbance spectral changes of R1 (a), R2 (b), R3 (c) and R4 (d) upon addition of 5 μL of different cations in CH_3CN:DMSO (v/v 9:1).

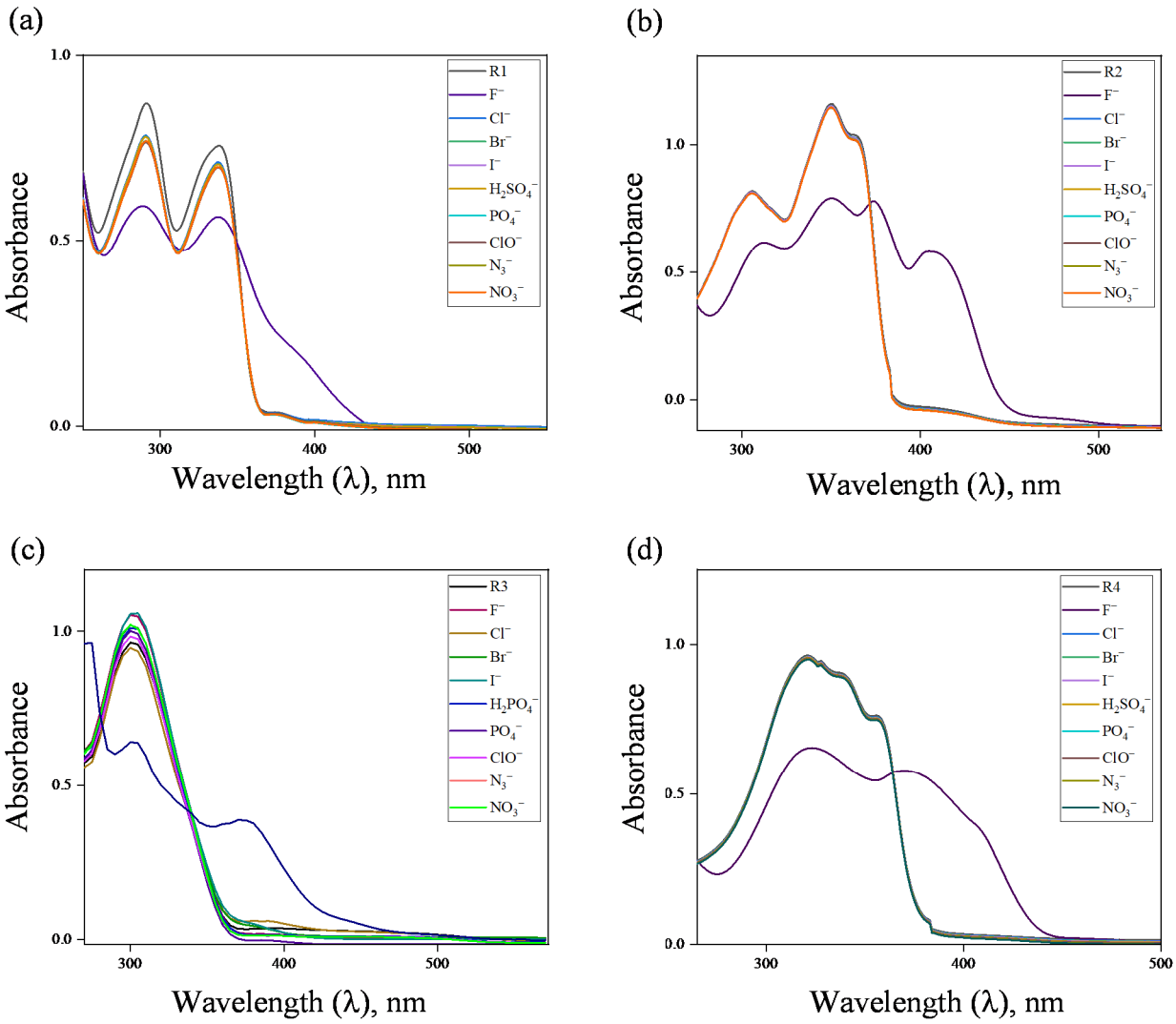

Fig. S17 Absorbance spectral changes of R1 (a), R2 (b), R3 (c) and R4 (d) upon addition of 5 μL of different anions in CH_3CN:DMSO (v/v 9:1).

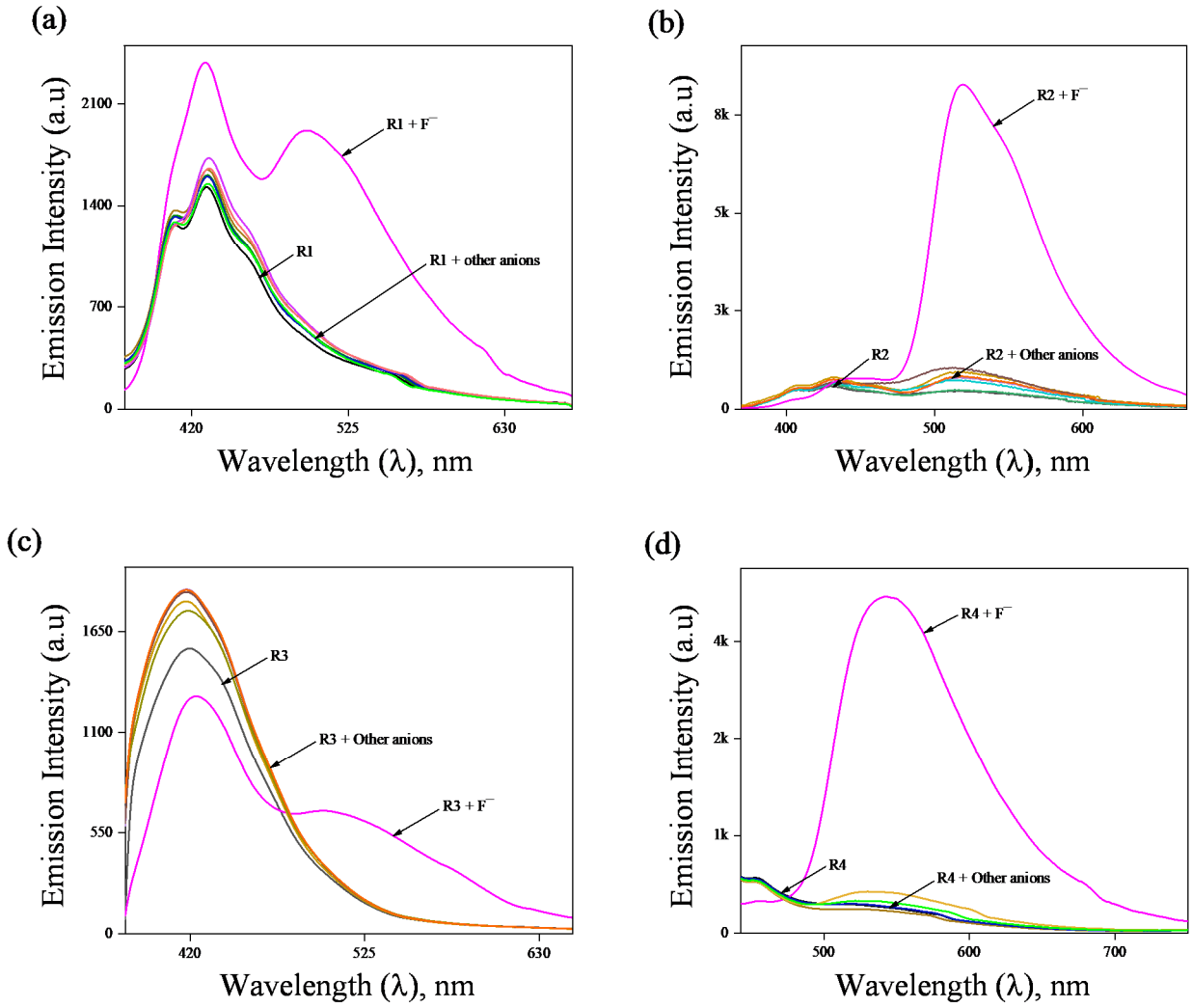

Fig. S18 Fluorescence spectral changes of R1 (a), R2 (b), R3 (c) and R4 (d) upon addition of 5 μL of different anions in CH_3CN:DMSO (v/v 9:1).

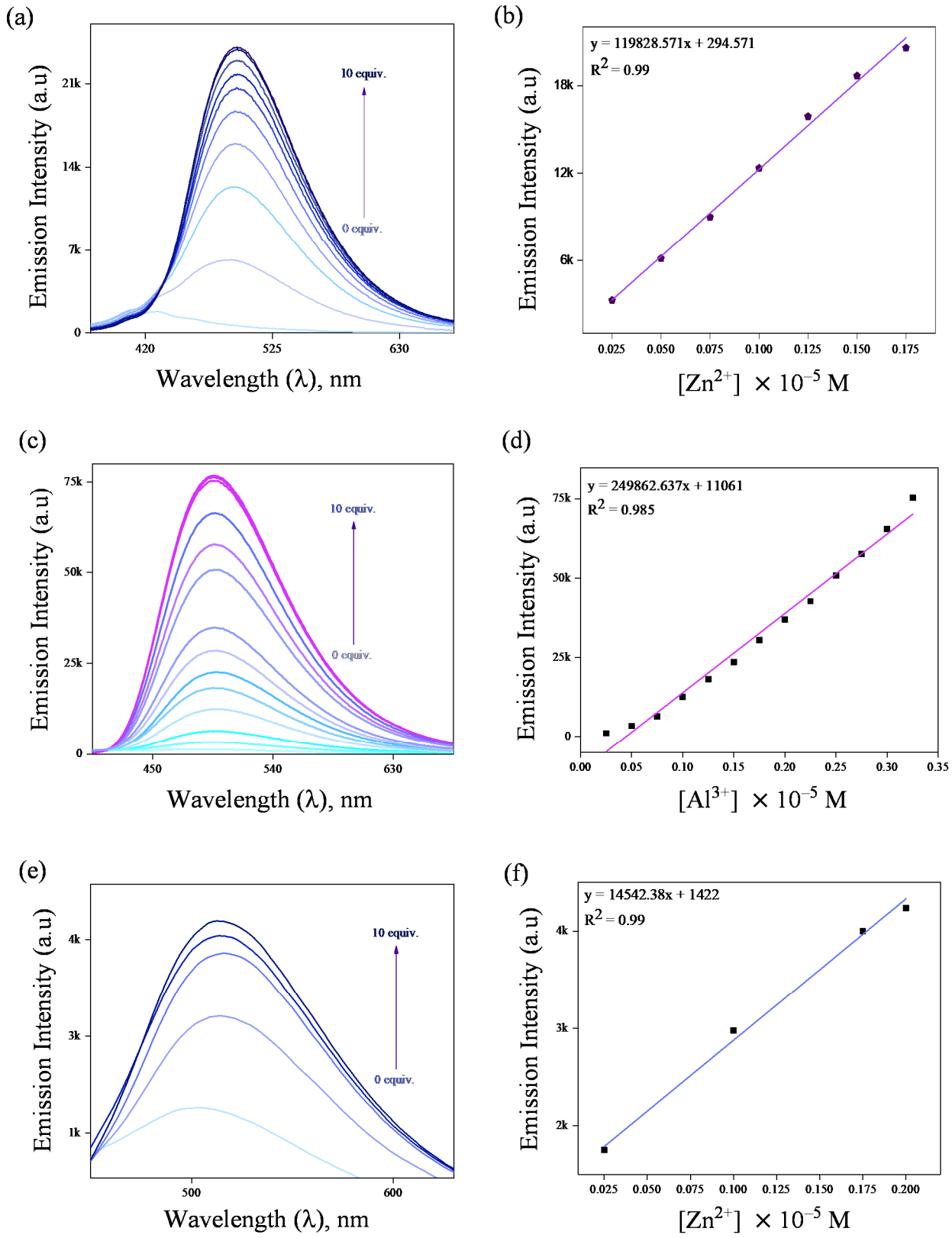

Fig. S19 Fluorescence spectral titrations of the chemosensor R3 on incremental addition of Zn^{2+} (a) and Al^{3+} (c) cations, and their corresponding calibration plots (b and d), and R4 on incremental addition of Zn^{2+} cation (e) and its corresponding calibration plot (f).

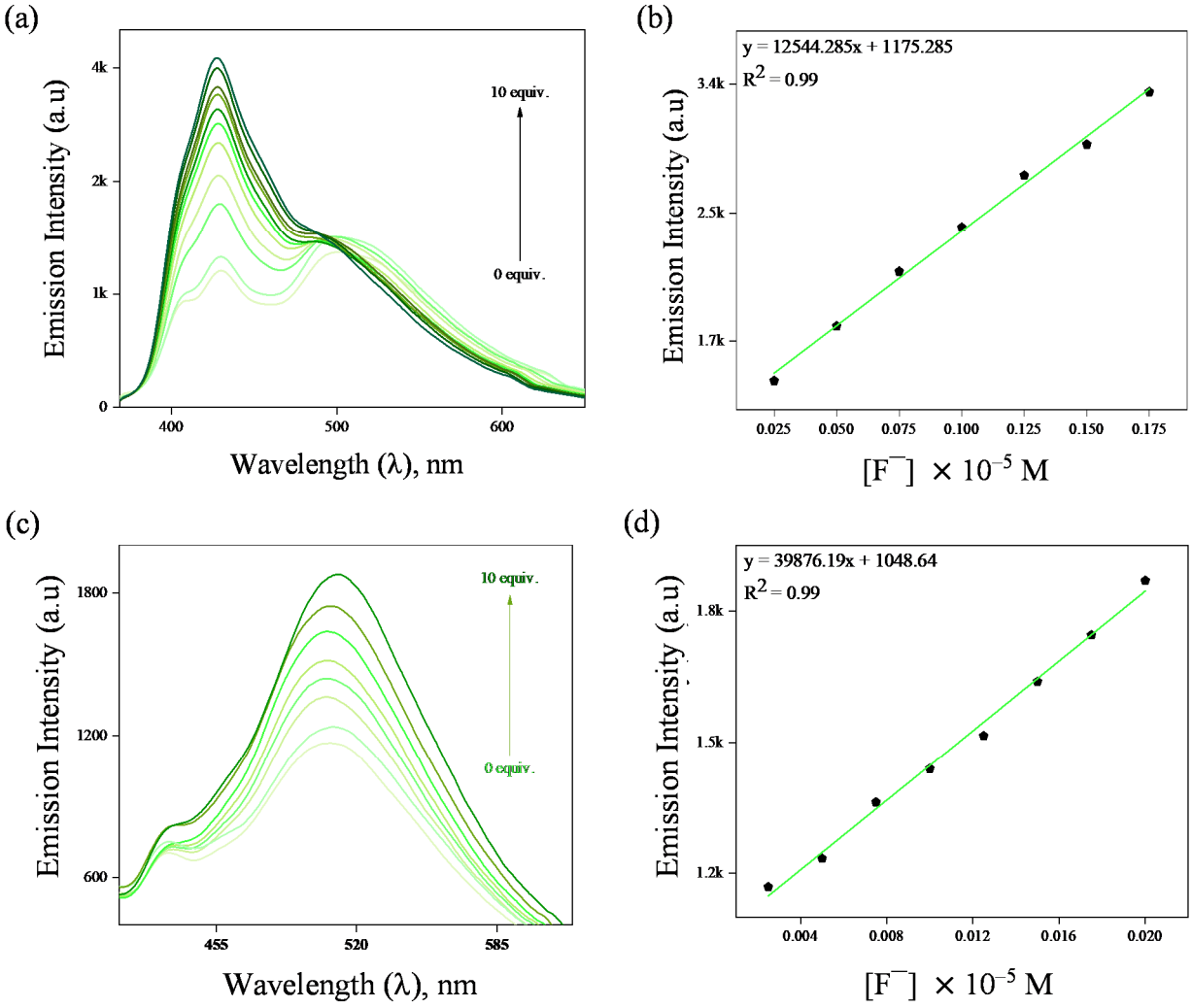

Fig. S20 Fluorescence spectral titrations of the chemosensors R1 (a) and R2 (c) on incremental addition of F^- anion, and their corresponding calibration plots (b and d).

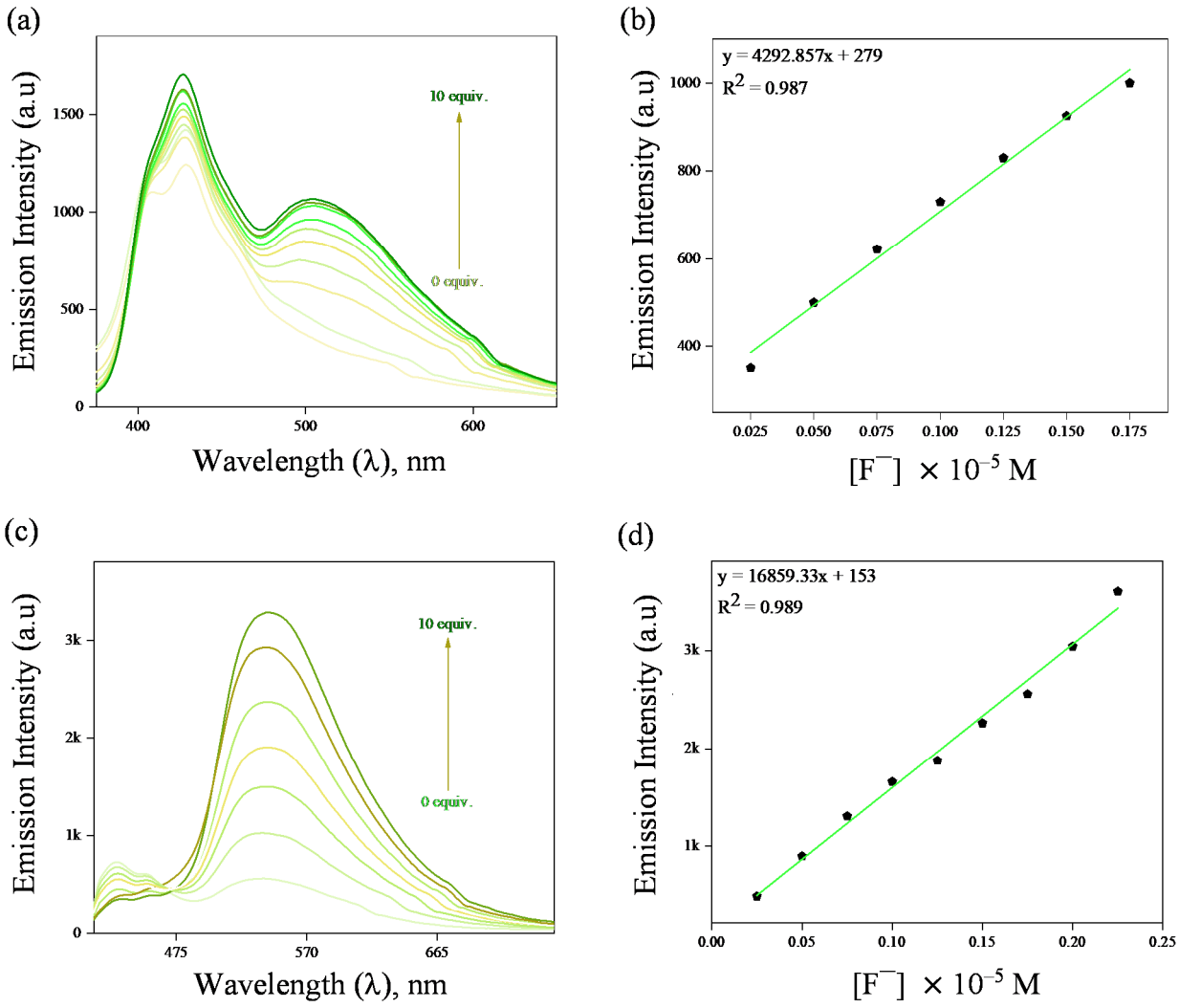

Fig. S21 Fluorescence spectral titrations of the chemosensors R3 (a) and R4 (c) on incremental addition of F^- anion and their corresponding calibration plots (b and d).

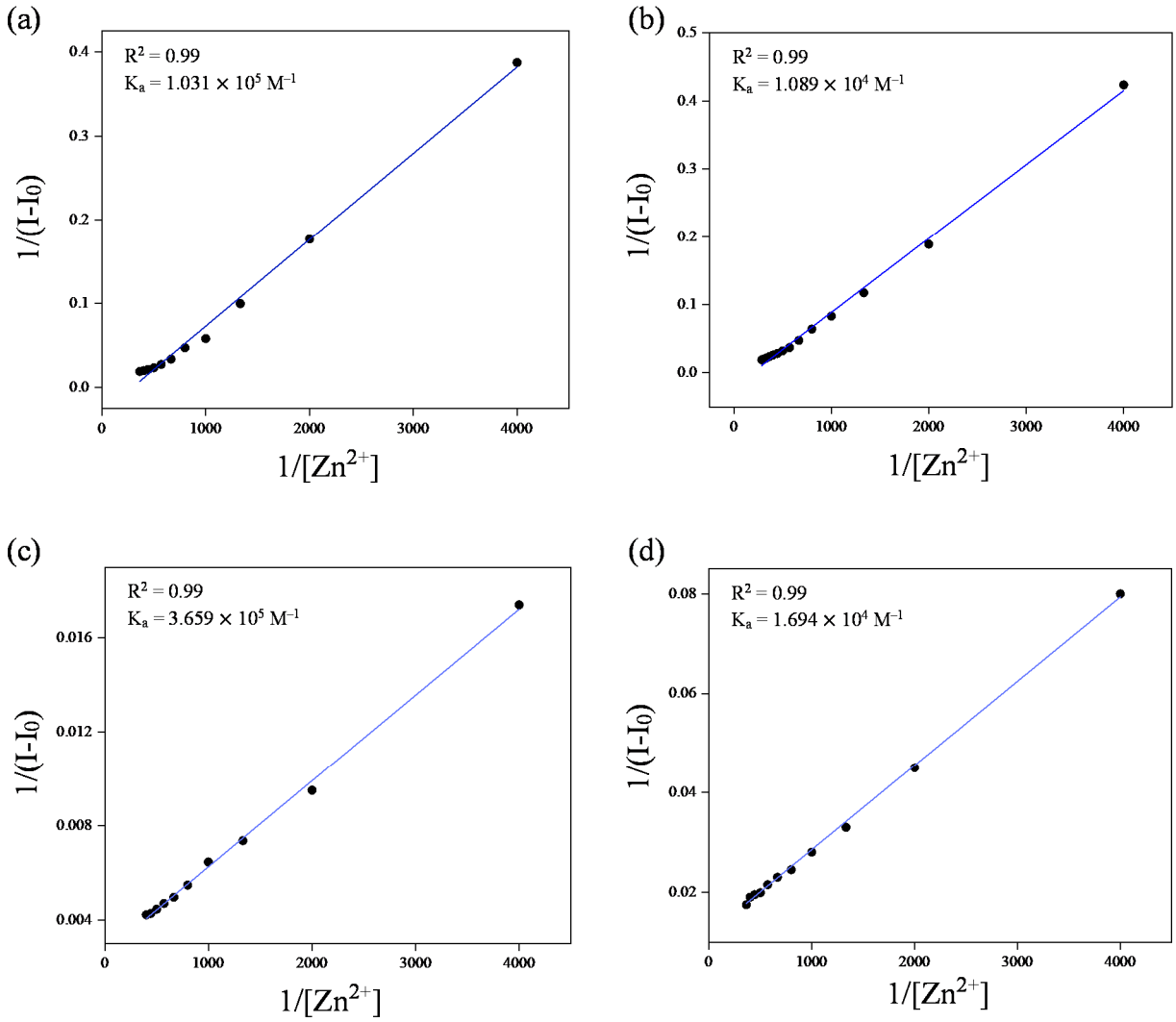

Fig. S22 Benesi-Hildebrand plots of the chemosensors R1 (a), R2 (b), R3 (c) and R4 (d) with Zn^{2+} cation for the calculation of association constant from fluorescence spectral titration studies.

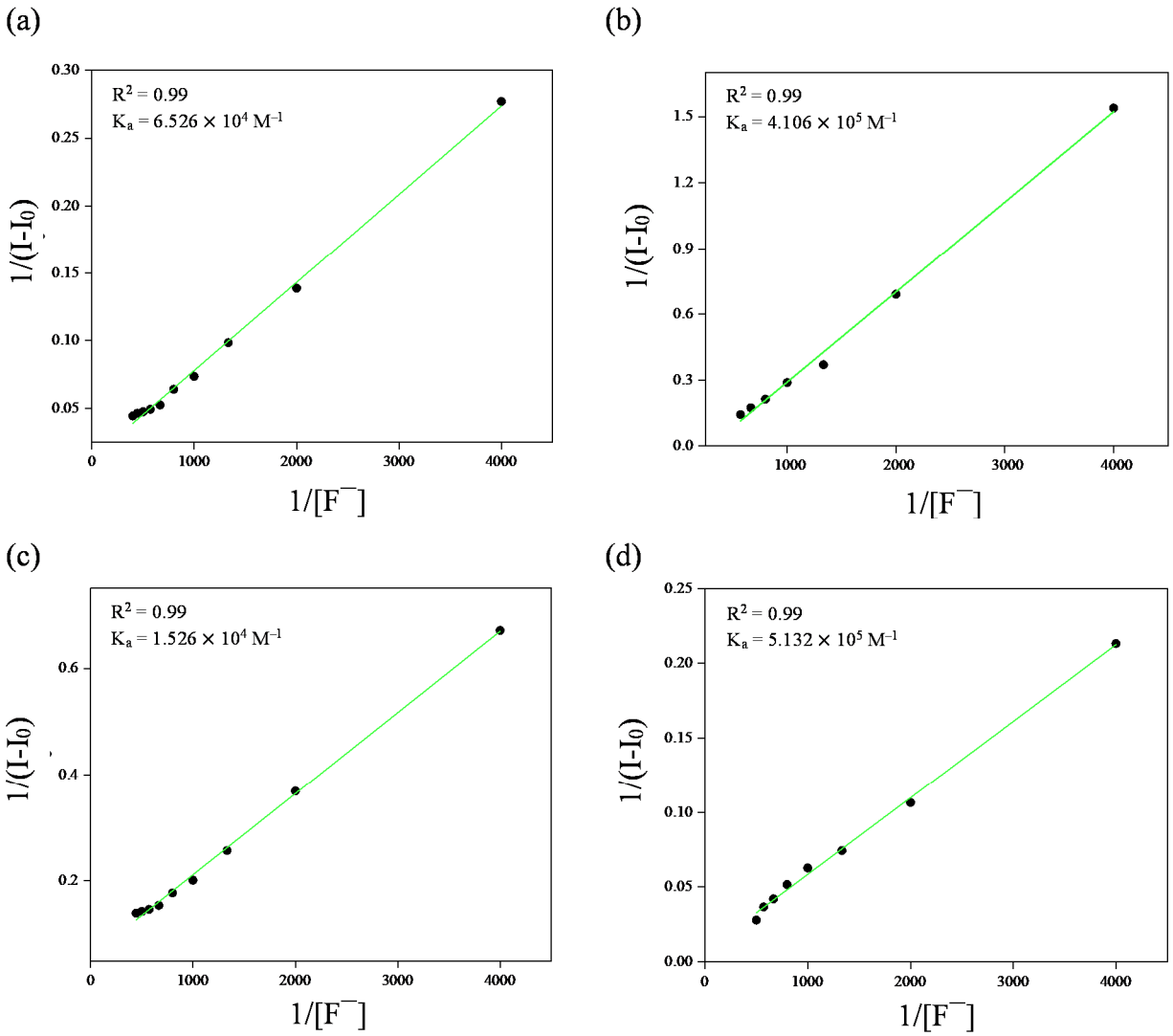

Fig. S23 Benesi-Hildebrand plots of the chemosensors R1 (a), R2 (b), R3 (c) and R4 (d) with F^-anion for the calculation of association constant from fluorescence spectral titration studies.

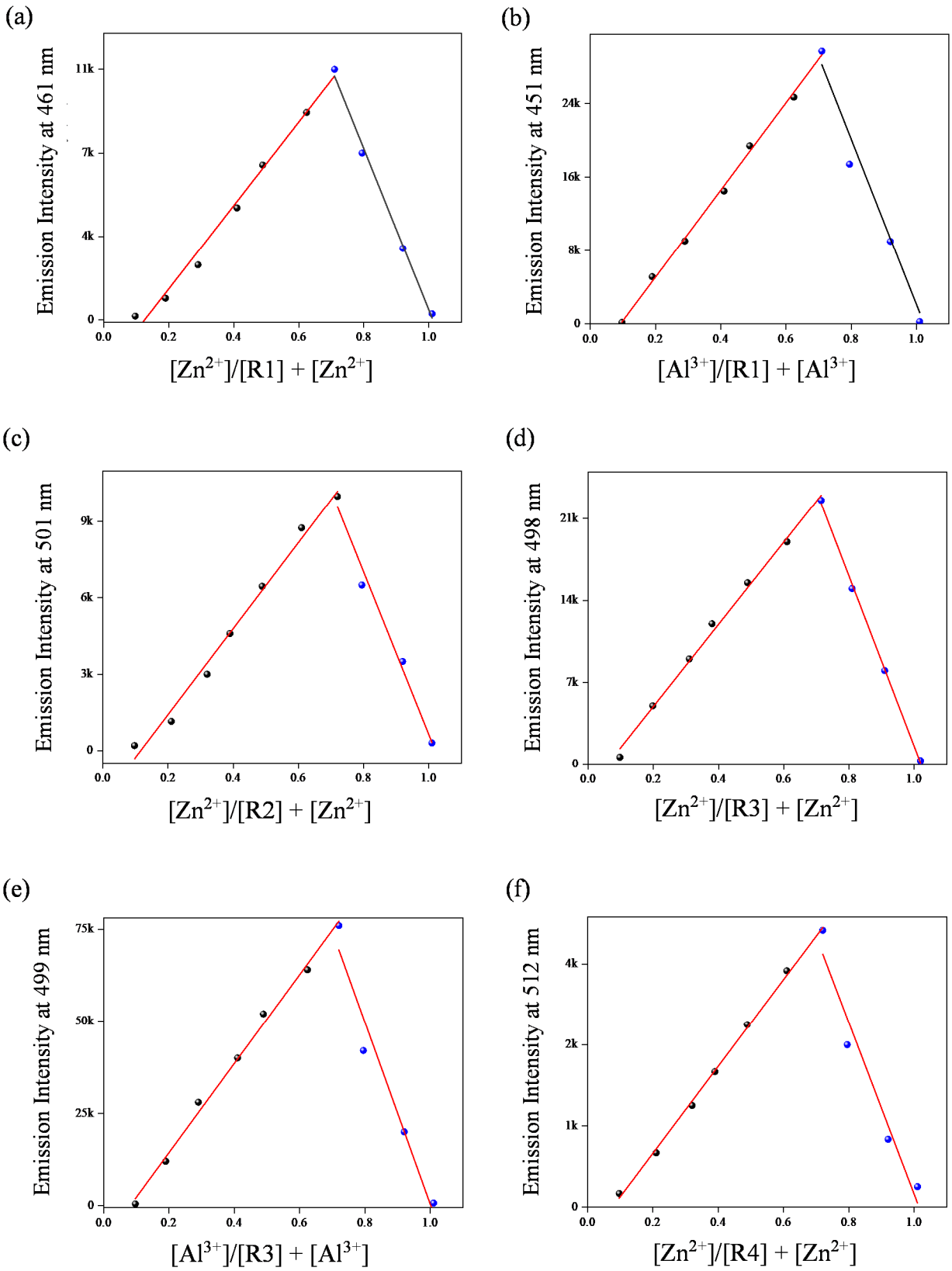

Fig. S24 Job´s plot analysis of the chemosensors (R1–R4) upon complexing with Zn^{2+} and Al^{3+} cations: R1 + Zn^{2+} (a), R1 + Al^{3+} (b), R2 + Zn^{2+} (c), R3 + Zn^{2+}, (d) R3 + Al^{3+} (e) and R4 + Zn^{2+} (f).

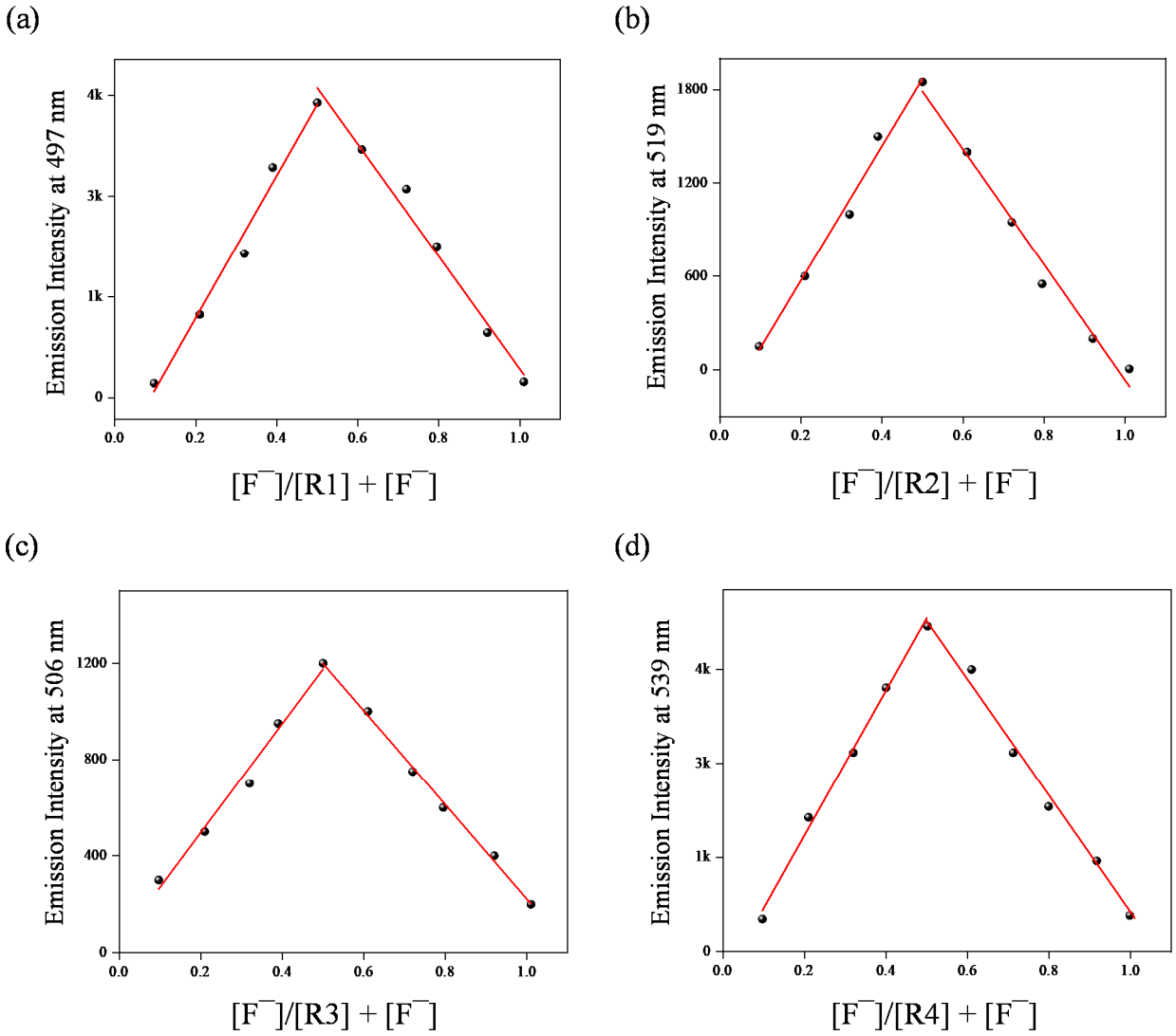

Fig. S25 Job´s plot analysis of the chemosensors (R1–R4) upon complexing with F^- anion: R1 + F^- (a), R2 + F^- (b), R3 + F^- (c) and R4 + F^- (d).

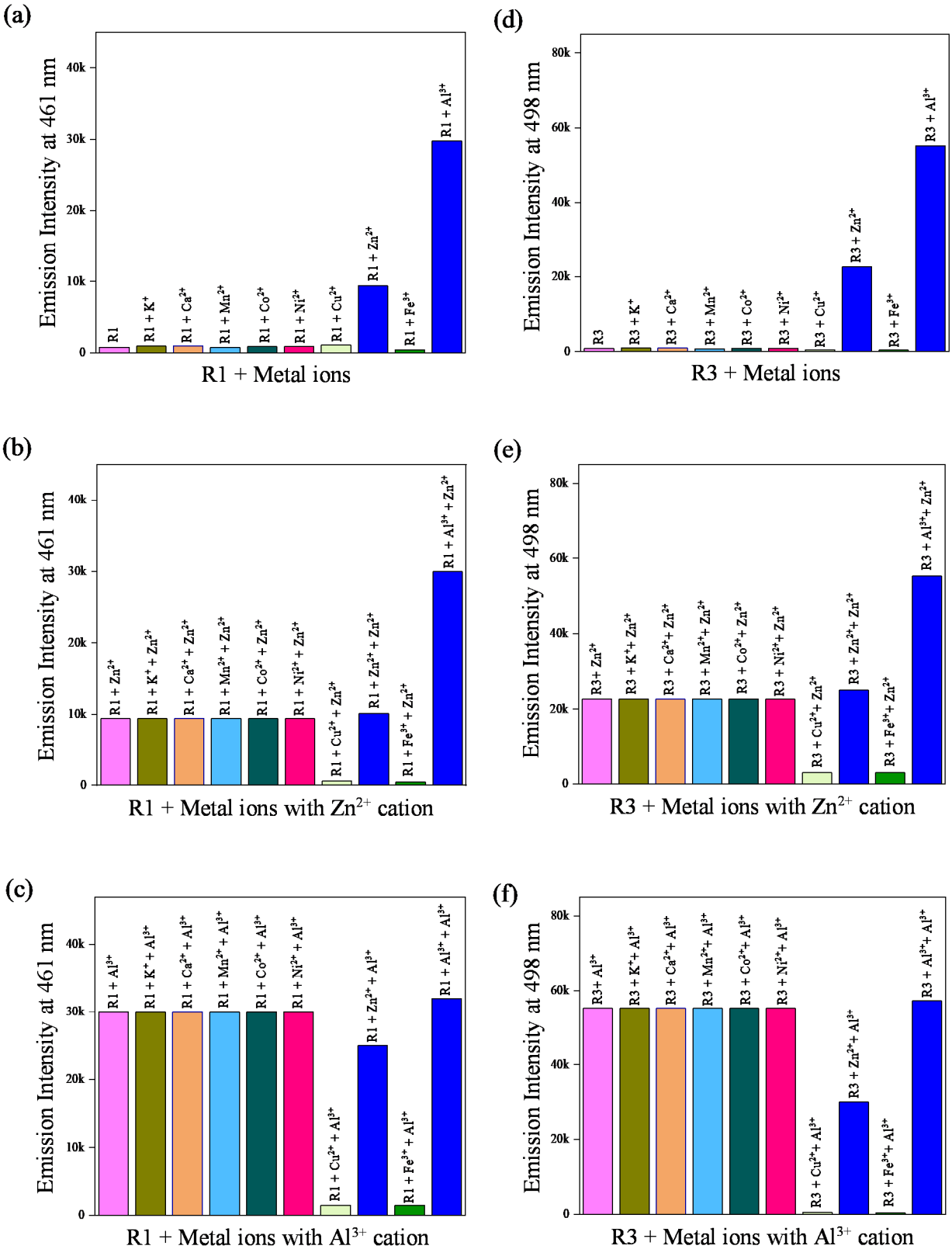

Fig. S26 Relative emission intensity as bar graph showing metal competition analysis of the chemosensors R1 and R3 with 10 equiv. of Zn^{2+} and Al^{3+} cations: R1 + Metal ions (a), R1 + Competing metal ions + Zn^{2+} (b), R1 + Competing metal ions + Al^{3+} (c), R3 + Metal ions (d), R3 + Competing metal ions + Zn^{2+} (e) and R3 + Competing metal ions + Al^{3+} (f), in CH_3CN:DMSO (v/v 9:1).

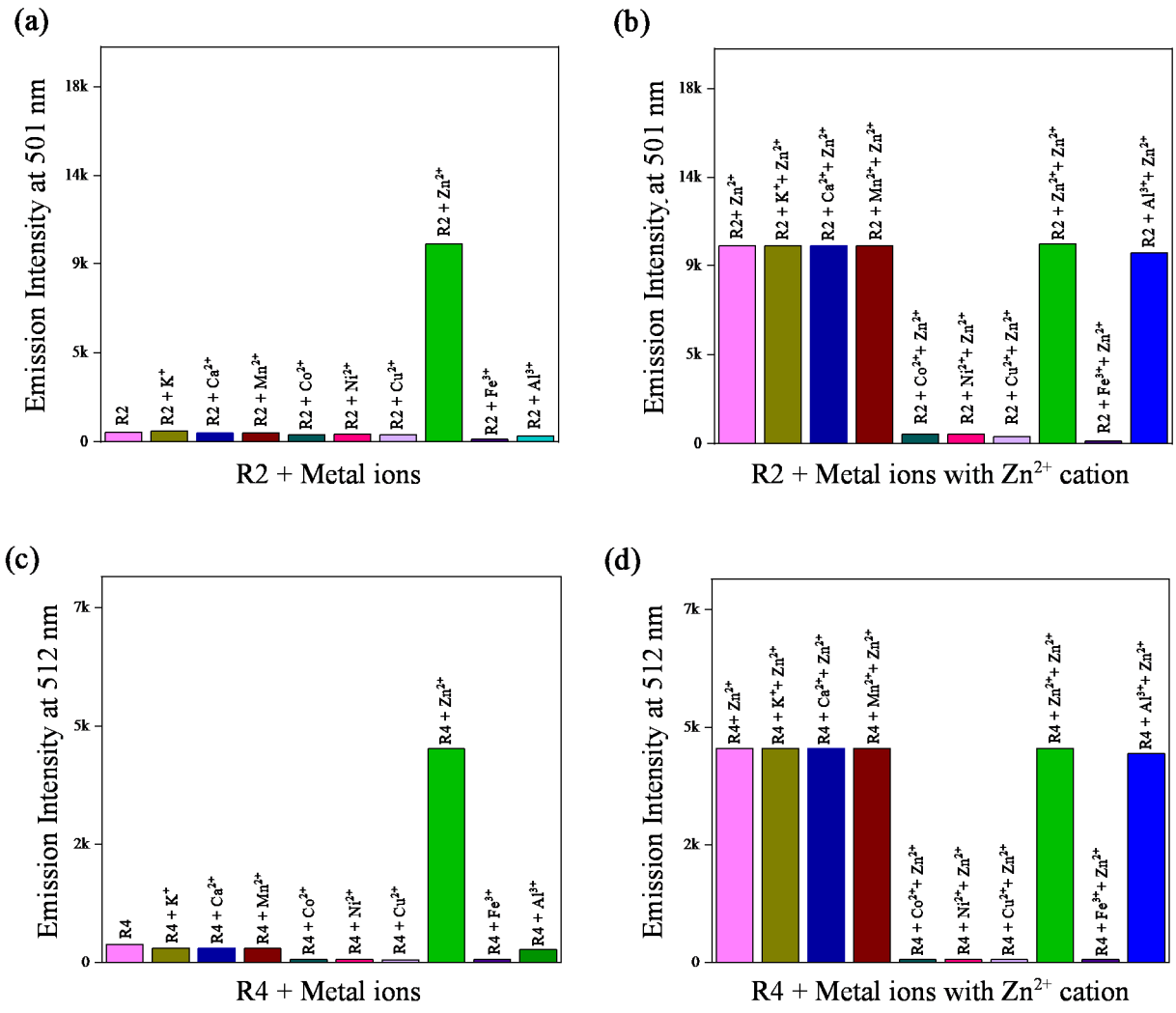

Fig. S27 Relative emission intensity as bar graph showing metal competition analysis of the chemosensors R2 and R4 with 10 equiv. of Zn^{2+} cations: R2 + Metal ions (a), R2 + Competing metal ions + Zn^{2+} (b), R4 + Metal ions (c) and R4 + Competing metal ions + Zn^{2+} (d), in CH_3CN:DMSO (v/v 9:1).

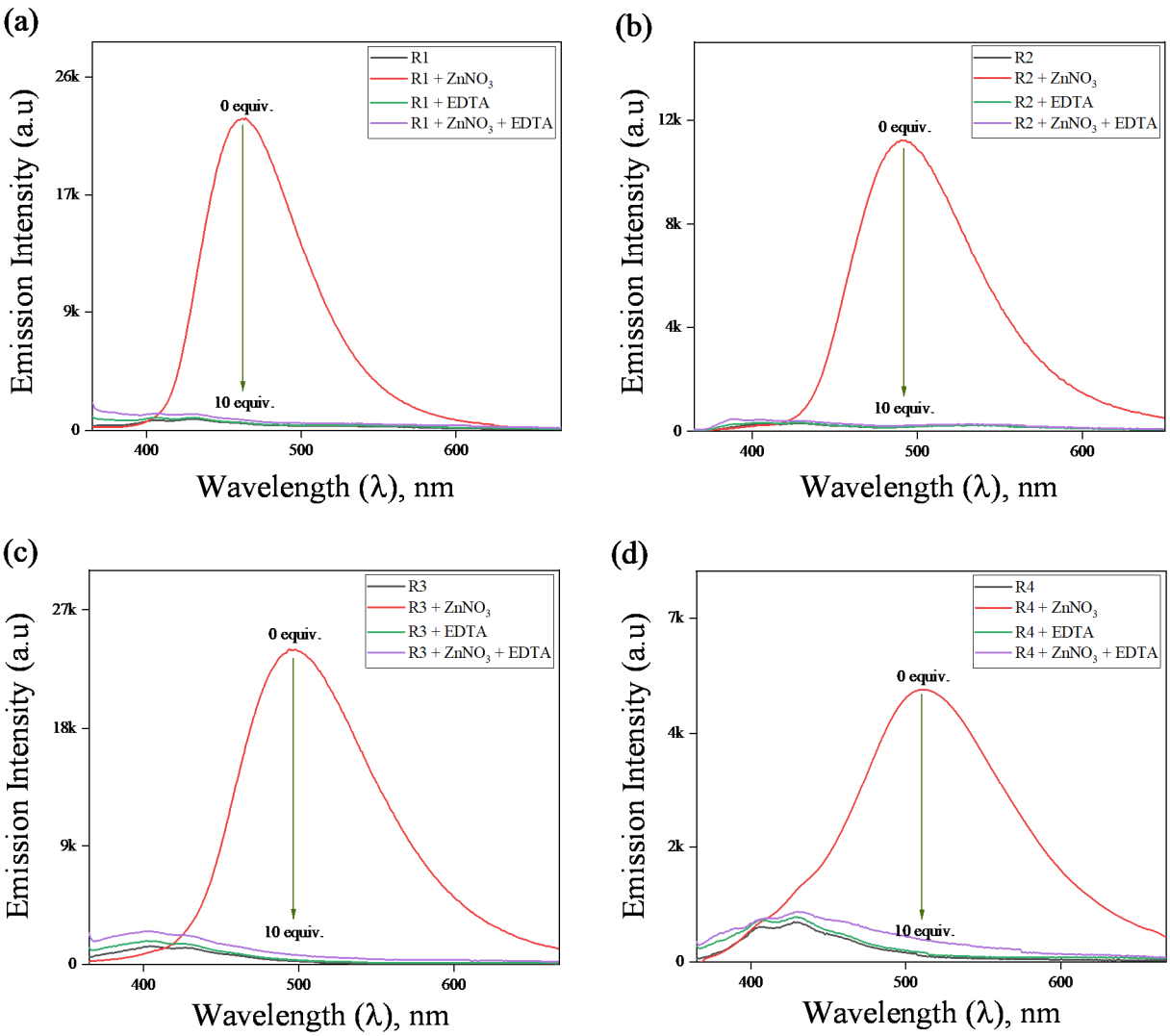

Fig. S28 Fluorescence reversibility responses of the chemosensors R1 (a), R2 (b), R3 (c) and R4 (d) upon alternate addition of Zn^{2+} and EDTA.

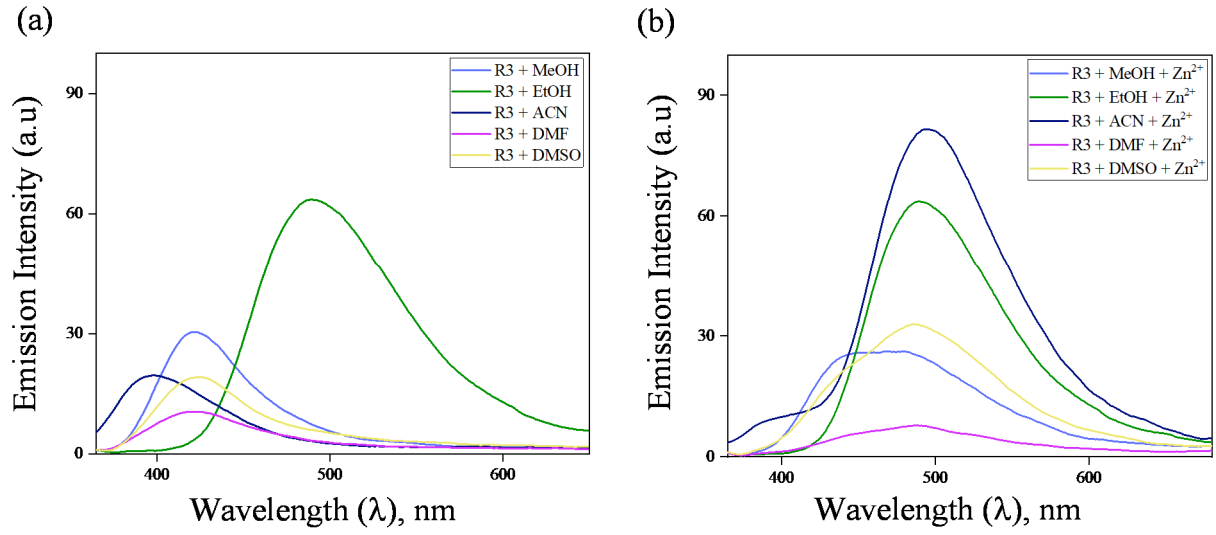

Fig. S29 Fluorescence spectral changes of the chemosensor R3 (a) and R3 in presence of Zn^{2+} cation (b), using different solvents.

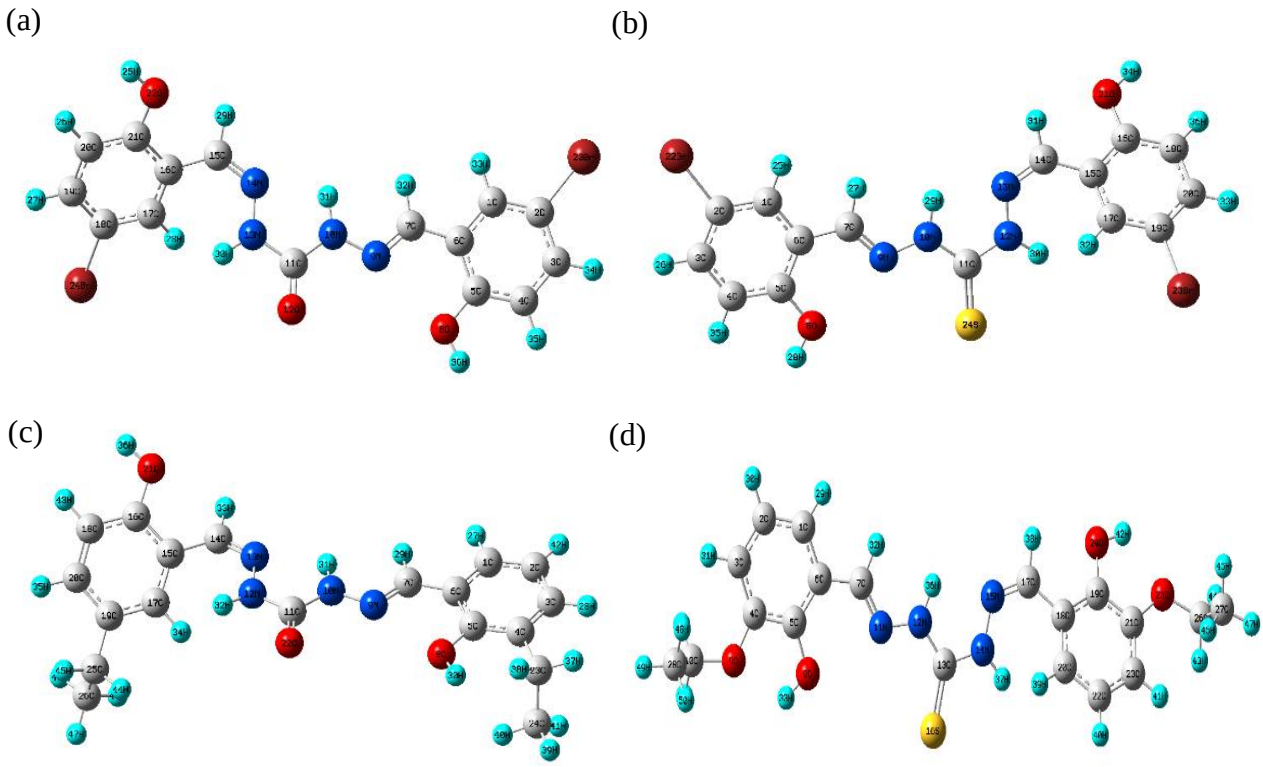

Fig. S30 The optimized structures of the chemosensors R1 (a), R2 (b), R3 (c) and R4 (d).

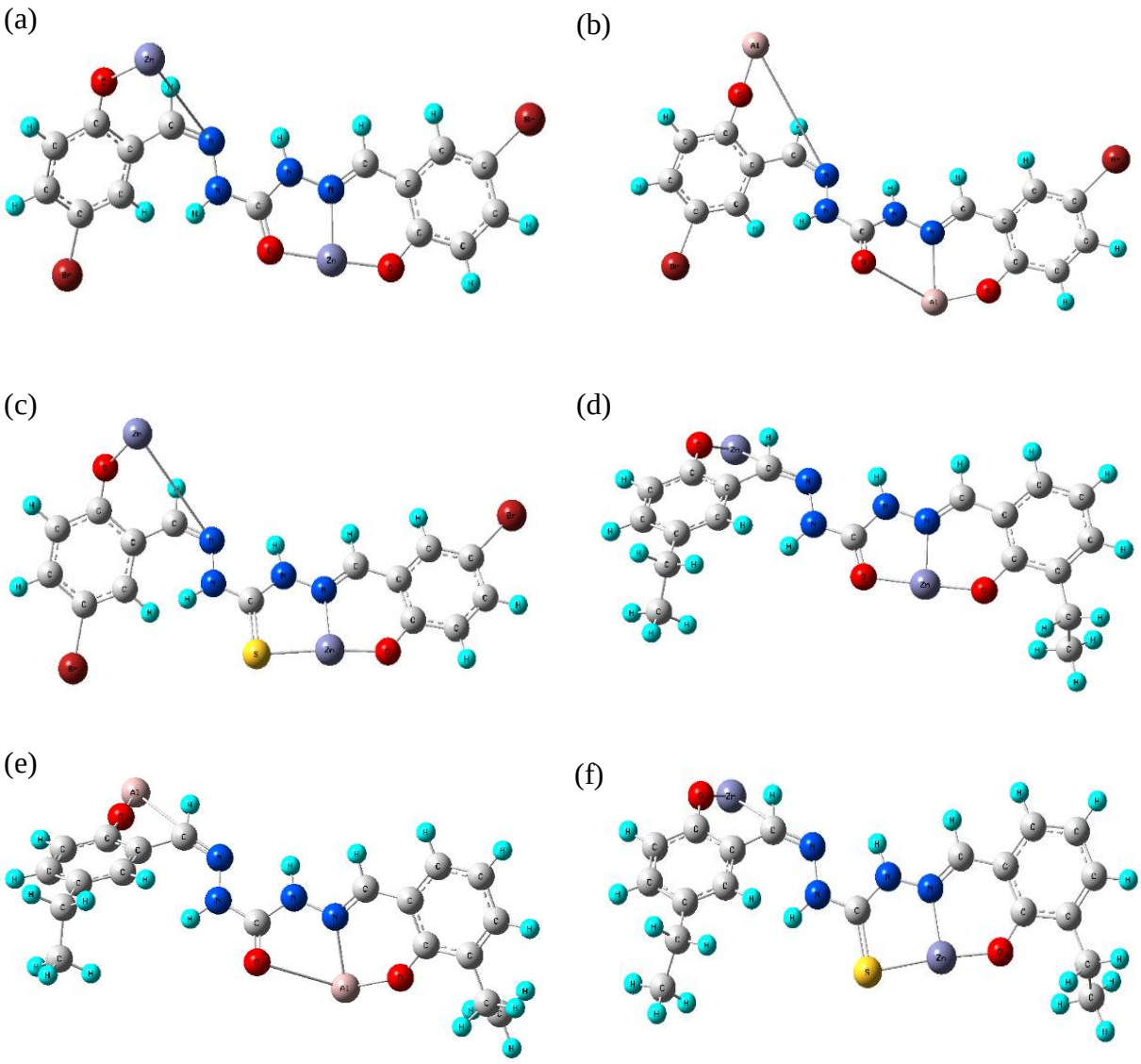

Fig. S31 The optimized structures of the chemosensors (R1–R4) upon binding with Zn^{2+} and Al^{3+} cations: R1 + Zn^{2+} (a), R1 + Al^{3+} (b), R2 + Zn^{2+} (c), R3 + Zn^{2+} (d) R3 + Al^{3+} (e) and R4 + Zn^{2+} (f).

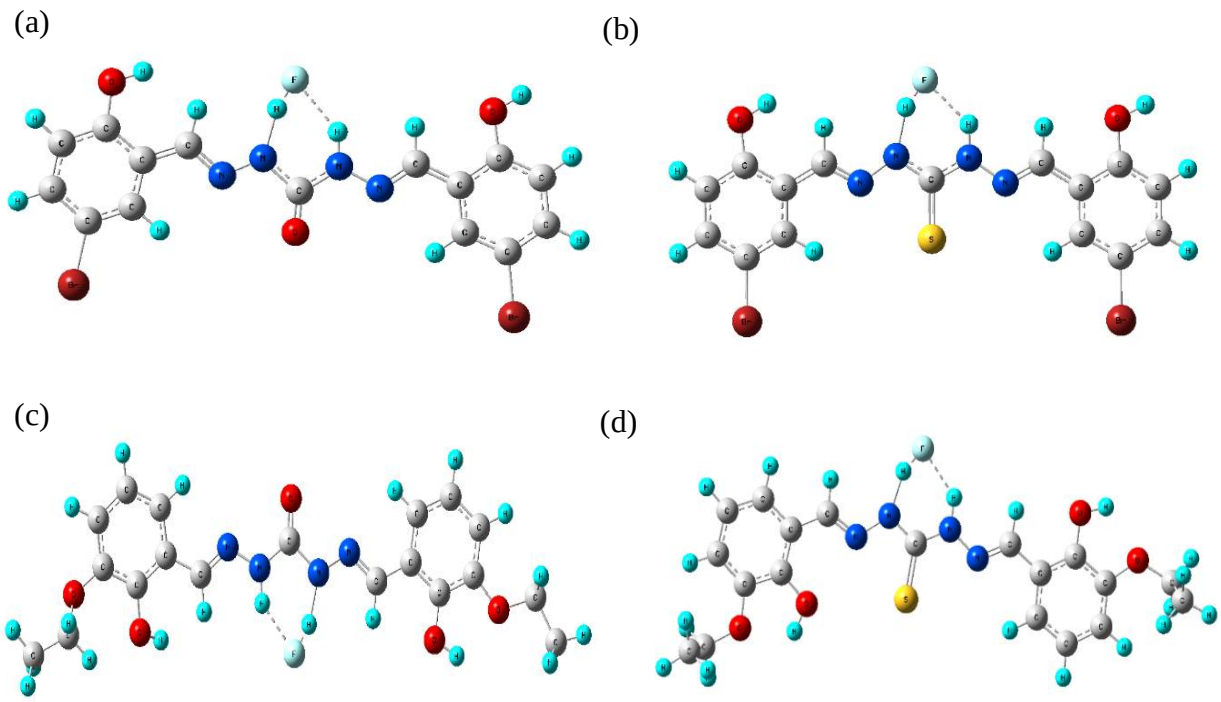

Fig. S32 The optimized structures of the chemosensors (R1–R4) upon binding with F^- anion: R1 + F^- (a), R2 + F^- (b), R3 + F^- (c) and R4 + F^- (d).

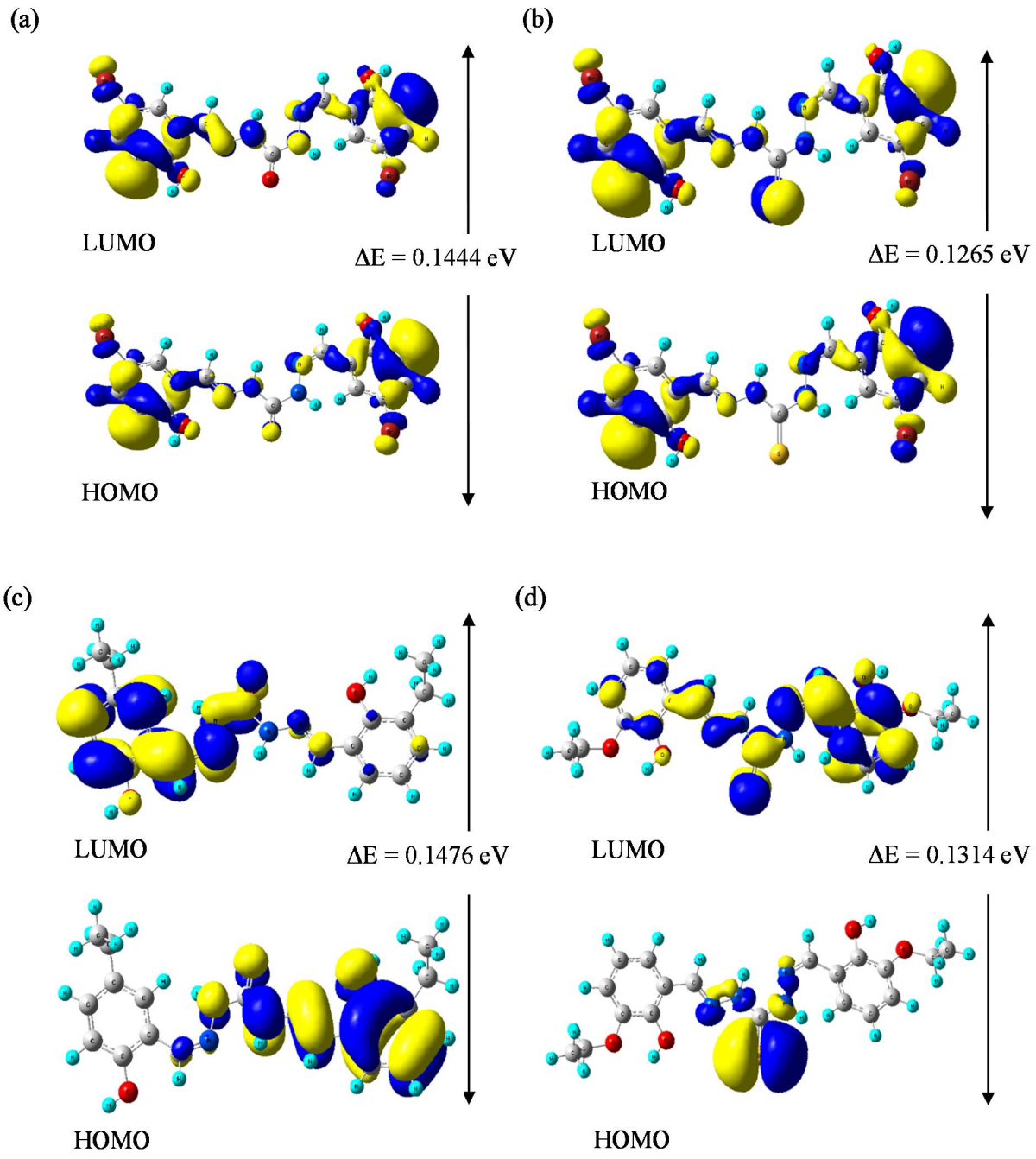

Fig. S33 Frontier molecular orbitals of the chemosensors R1 (a), R2 (b), R3 (c) and R4 (d).

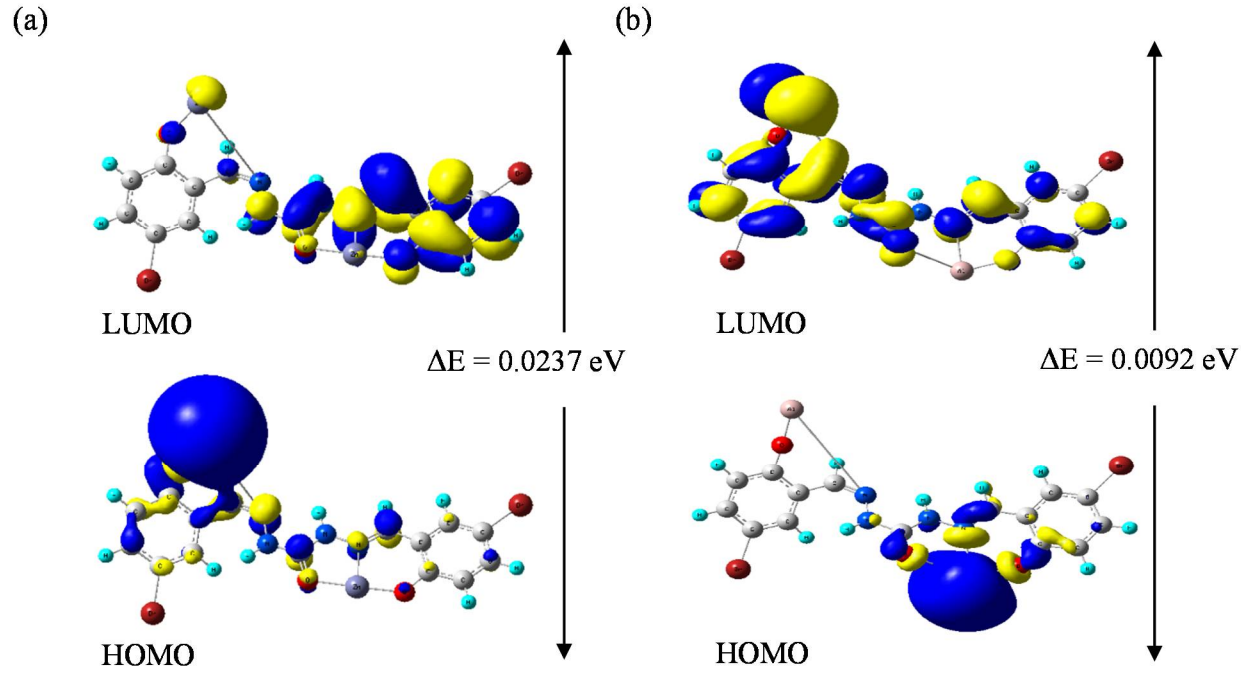

Fig. S34 Frontier molecular orbitals of the chemosensor R1 upon binding with Zn^{2+} and Al^{3+} cations: R1 + Zn^{2+} (a) and R1 + Al^{3+} (b).

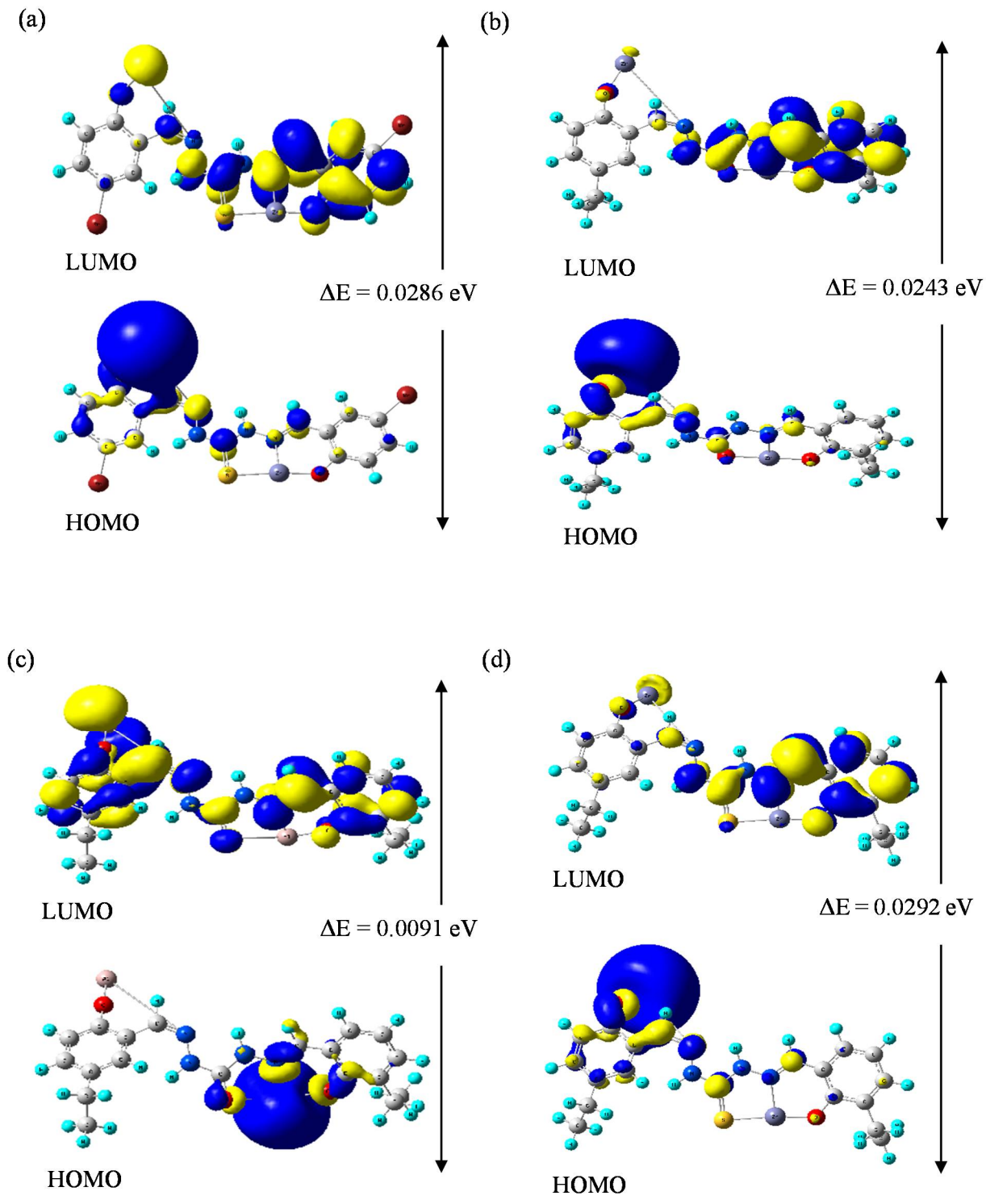

Fig. S35 Frontier molecular orbitals of the chemosensors R2, R3 and R4 upon binding with Zn^{2+} and Al^{3+} cations: R2 + Zn^{2+} (a), R3 + Zn^{2+} (b), R3 + Al^{3+} (c) and R4 + Zn^{2+} (d).

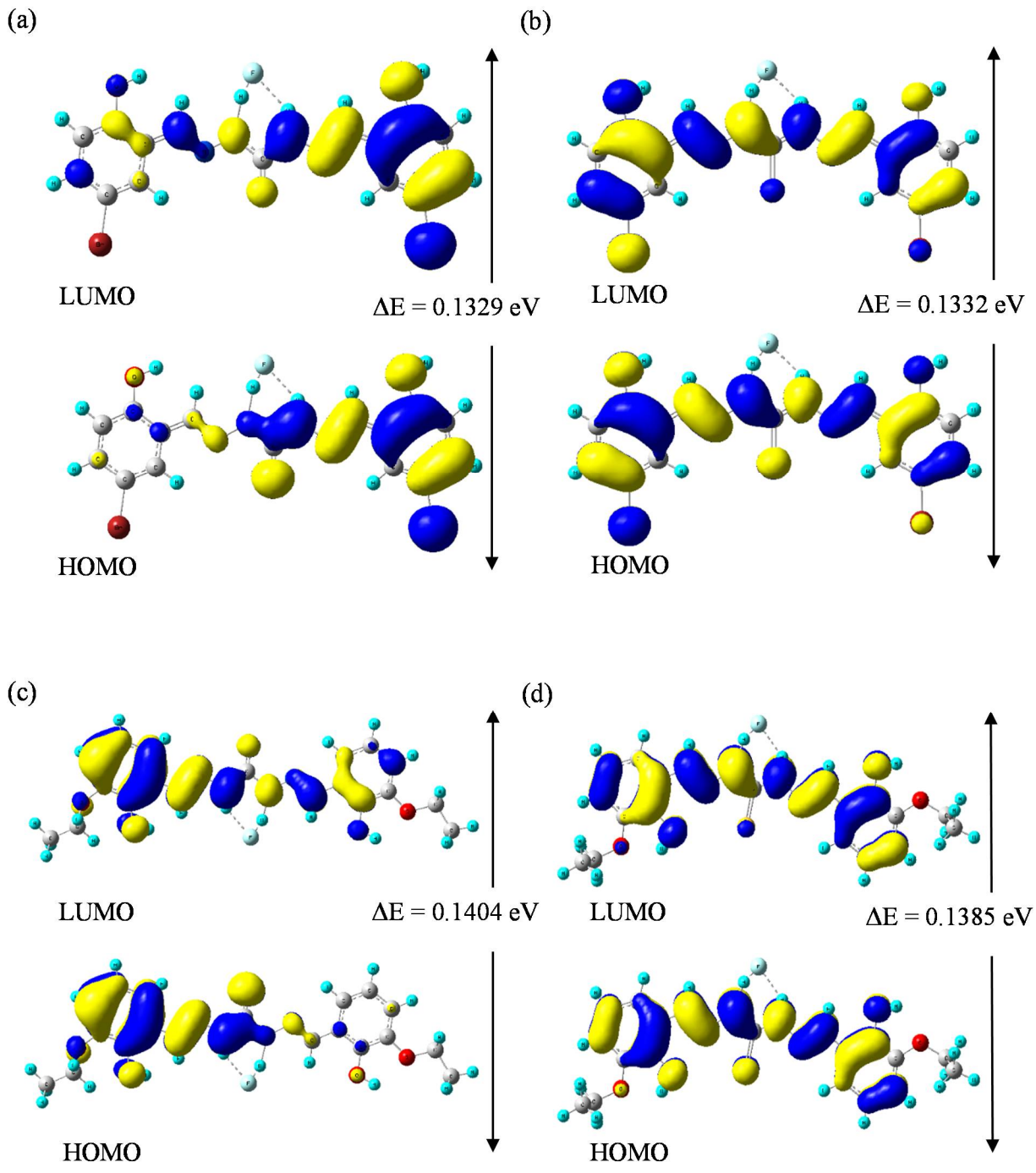

Fig. S36 Frontier molecular orbitals of the chemosensors (R1–R4) upon binding with F^- anion: R1 + F^- (a), R2 + F^- (b), R3 + F^- (c) and R4 + F^- (d).

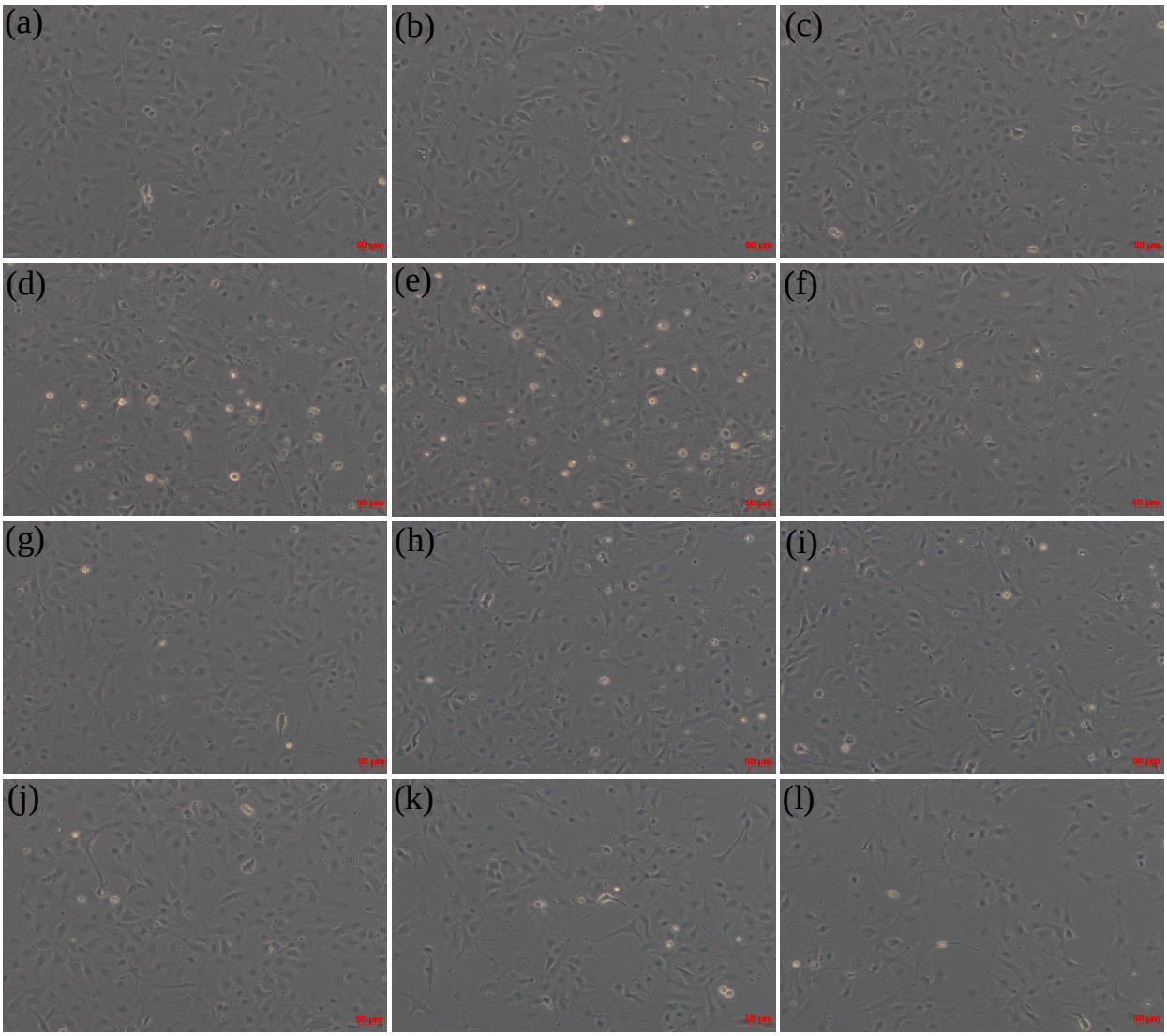

Fig. S37 Morphological alteration of *Dr*G cell lines exposed to various concentrations of R1 and R3 for 24 h: Control cells (a), cells exposed to 20 µM of R1 (b), cells exposed to 40 µM of R1 (c), cells exposed to 60 µM of R1 (d), cells exposed to 80 µM of R1 (e) and cells exposed to 100 µM of R1 (f); Control cells (g), cells exposed to 20 µM of R3 (h), cells exposed to 40 µM of R3 (i), cells exposed to 60 µM of R3 (j), cells exposed to 80 µM of R3 (k) and cells exposed to 100 µM of R3 (l); Images captured at 100 × magnification.

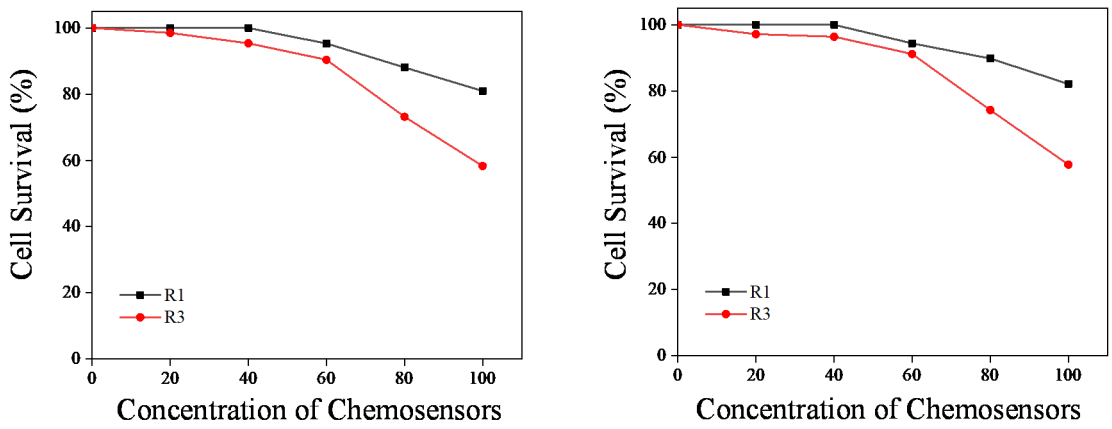

Fig. S38 *In vitro* cytotoxicity of the chemosensors R1 and R3 on *Dr*G cell lines after 24 h exposure by MTT (a) and NR uptake (b) assays; The individual data points are expressed as the arithmetic mean percentage of control (mean ± SE; n = 8 replicate).